JOURNAL OF PLANKTON RESEARCH | VOLUME 24 | NUMBER 3 | PAGES 167–189 | 2002

# The flow field around a freely swimming copepod in steady motion. Part I: Theoretical analysis

**HOUSHUO JIANG[1,4], THOMAS R. OSBORN[1,3] AND CHARLES MENEVEAU[2,3]**

[1]DEPARTMENT OF EARTH AND PLANETARY SCIENCES, [2]DEPARTMENT OF MECHANICAL ENGINEERING, [3]CENTER FOR ENVIRONMENTAL AND APPLIED FLUID MECHANICS, THE JOHNS HOPKINS UNIVERSITY, BALTIMORE, MD 21218, USA

[4]CURRENT ADDRESS: MS #9, DEPARTMENT OF APPLIED OCEAN PHYSICS AND ENGINEERING, WOODS HOLE OCEANOGRAPHIC INSTITUTION, WOODS HOLE, MA 02543, USA

CORRESPONDING AUTHOR: H. JIANG. E-MAIL: hsjiang@whoi.edu

*The three-dimensional flow field around a free-swimming copepod in steady motion was studied theoretically. This study was based on coupling the Navier–Stokes equations with the dynamic equations for an idealized body of a copepod. To allow analytical solutions to the flow field, three simplifications were made: (a) to simulate the effect of the beating movement of the cephalic appendages, a force-field was added to the Navier–Stokes equations, (b) to linearize the problem, Stokes flow was used, and (c) to simplify the morphologies of the copepods, a spherical body shape was assumed. Analytical solutions were derived for five steady motions: (1) hovering, (2) sinking, (3) upwards swimming, (4) backwards swimming and (5) forwards swimming. The results show that the geometry of the flow field around a freely swimming copepod varies significantly with the different swimming behaviours. When a copepod hovers in the water, or swims very slowly, it generates a wide, cone-shaped flow field. In contrast, when a copepod sinks, or swims fast, the flow geometry is not cone-shaped, but cylindrical, narrow and long. These results are consistent with published observations on live copepods. It is shown that the differences in the flow geometry with the different swimming behaviours are due to the relative importance between the two factors in generating the flow field: the copepod's swimming motion and the requirement to counterbalance the copepod's excess weight. The results also highlight the importance of considering freely swimming copepods as self-propelled rather than as towed bodies. 'Self-propelled' means a freely swimming copepod must gain thrust from the surrounding water in order to counterbalance the drag force by water and its excess weight. Regardless of swimming behaviours and velocities, the far-field velocity field decays to that of the velocity field generated by a point force of magnitude equal to the copepod's excess weight in an infinite domain. On the other hand, using the towed body model yields a flow field with much different far- and near-field flow characteristics. Hence, the towed body model is inherently unable to reproduce fundamental characteristics of the flow field around a freely swimming copepod.*

## INTRODUCTION

### Historical background

The first investigator to conceive of the idea that calanoid copepods generate a feeding current was Esterly (Esterly, 1916), who described food particles streaming towards the mouth from behind, through a funnel formed by the maxillae. However, he was unable to observe the rapid movements of the cephalic appendages and did not know how this stream was produced.

Storch and Pfisterer described the feeding mechanism of *Diaptomus gracilis*, a freshwater calanoid copepod species (Storch and Pfisterer, 1925). They described how the food particles were filtered by the long setae of the maxillae from a current of water passing through them from behind. It was postulated that the beating movement of the cephalic appendages produced a strong current

flowing from anterior to posterior along the ventral side of the body. This current, consequently directed by the cephalic appendages from antennae (the longest) to maxillules (the shortest), is drawn closer to the body and guided by the maxillulary epipod. After flowing rapidly backwards over the antero-lateral surface of the maxillae, the water current is finally sucked out through the maxillary setae that are replaced from behind.

Some of the views of Storch and Pfisterer (Storch and Pfisterer, 1925) were strongly criticized by Cannon (Cannon, 1928) who observed the currents produced by *Calanus finmarchicus* and by *Diaptomus gracilis* 'swimming' in a drop of water under a microscope. Cannon's observations agreed with those of Storch and Pfisterer in that *Diaptomus gracilis* (as well as *Calanus finmarchicus*) feeds automatically when swimming slowly and steadily through the water. They also agreed that a feeding current is produced by the swimming activities of the anterior limbs and filtered by the stationary maxillae and that food so obtained is passed on to the mandibles by the maxillulary endites and setae on the bases of the maxillipeds. On the other hand, Cannon's observations did not show that there was a powerful antero-posterior swimming current, instead there were two large swirls, one on either side of the body in the angle between the antennule and the axis of the body. The swirls rotate in such a way that the water nearest the body moves backwards. The copepod thus moves steadily forwards in the middle of a vortex of moving water, which Cannon termed as the 'swimming vortex'. It was also shown that there was a secondary, smaller vortex inside the swimming vortex, rotating in the opposite direction. The secondary vortex carries food particles forward to the maxillae and is termed the 'feeding vortex'. Cannon believed that both vortices resulted automatically from the swimming activities of the antennae, mandibular palps and maxillules.

Lowndes (Lowndes, 1935) did a considerable amount of experimental work, including the use of the polygraph and instantaneous photomicrography, to study as many as ten species of copepods. His results showed that the feeding of calanoid copepods was neither automatic nor non-selective and differed considerably from species to species. Gauld (Gauld, 1966) continued the work by Lowndes (Lowndes, 1935) and Cannon (Cannon, 1928) and further compared the morphological differences between species in order to relate them to the feeding mechanisms. It has been suggested that a double-acting stroke of the antennae, in which the endopods and exopods of the antennae beat alternately, produces the smooth, gliding movement characteristic of the genera—*Calanus*, *Pseudocalanus*, *Euchaeta*, *Centropages*, *Isias*, *Temora*, *Diaptomus* and *Eurytemora*. Comparatively, a simple paddling stroke produces a jerky motion in a few other calanoids—*Anomalocera* and *Acartia*, and in cyclopoids, such as *Oithona*.

Most of the above-mentioned authors actually believed that the calanoid copepods were 'filter-feeders' and what they had debated on was how copepods filtered algae from the water. For a long time, many calanoid copepods had been described as 'filter-feeders', i.e. 'feeding passively by passing the surrounding water through structures that retain particles according to size and shape' as defined by Jørgensen (Jørgensen, 1966).

Until high-speed microcinematography was used to observe adult females of *Eucalanus crassus* and *Eucalanus pileatus* feeding in 120 ml of sea water (Alcaraz *et al.*, 1980; Koehl and Strickler, 1981; Strickler, 1982; Paffenhöfer *et al.*, 1982), the researchers had concluded that the calanoid copepods were 'suspension-feeders'. 'They (the copepods) capture and handle the food particles not passively according to size and shape but, in most cases, actively using sensory inputs for detection, motivation to capture, and ingestion' (Paffenhöfer *et al.*, 1982). The vortices observed by Cannon (Cannon, 1928) have been proved to be artificial due to the effects of the wall and surface enclosing the small drop of water (Alcaraz *et al.*, 1980; Koehl and Strickler, 1981; Yule and Crisp, 1983). These authors generally observed that the combined movements of the cephalic appendages propel water and transport food particles towards the copepod, and generate a feeding current. They have also identified the low Reynolds number property of the feeding current. In this environment of low Reynolds numbers, the cephalic appendages of copepods employ the 'fling and clap' mechanism to direct and trap the food particles (Strickler, 1984). Living in a nutritionally dilute environment (Conover, 1968), the calanoid copepods are usually negatively buoyant, the reason for which can be found in an analysis of the forces acting upon a free-swimming calanoid copepod (Strickler, 1982).

From the early 1980s, the feeding currents generated by copepods have been intensively studied. In order to quantify the characteristics of a feeding current, one needs to know the velocity field of the feeding current. The laser-illuminated video-imaging technique can determine the three-dimensional coordinates of particles following the flow and then allow researchers to reconstruct the velocity field from the coordinates. Much work has been done with this technique, providing quantitative information about the feeding currents (Strickler, 1982; Cowles and Strickler, 1983; Price *et al.*, 1983; Vanderploeg and Paffenhöfer, 1985; Price and Paffenhöfer, 1986a; Paffenhöfer and Lewis, 1990; Jonsson and Tiselius, 1990; Tiselius and Jonsson, 1990; Yen *et al.*, 1991; Yen and Fields, 1992; Bundy *et al.*, 1993; Fields and Yen, 1993, 1997; Bundy and Paffenhöfer, 1996; Yen and Strickler, 1996). In addition,

the laser sheet particle image velocimetry (PIV) technique has been used to obtain the instantaneous flow field around a copepod (Stamhuis and Videler, 1995; van Duren *et al.*, 1998). Recently, direct numerical simulation has been used to compute the feeding current around a tethered copepod, demonstrating that direct numerical simulation of the feeding current around a copepod is possible (Jiang *et al.*, 1999).

### Swimming behaviours of copepods

Generally, in calanoid copepods, there are two distinct forms of swimming behaviours (Lowndes, 1935). The first is the behaviour of swimming fast or jumping, which is performed faster than other activities and always involves strokes of the antennules and sometimes the swimming legs. This form of swimming is usually an escape reaction of copepods to take them away from the stimulus causing it. The second form is the slow-swimming behaviour (Gauld, 1966), resulting from the high-frequency beating of the paired cephalic appendages, the antennae, mandibular palps, maxillules, maxillae and maxillipeds. For most calanoid copepods, the behaviour of swimming slowly is closely connected with another behaviour of these copepods, i.e. generating a feeding current, since both behaviours utilize the cephalic appendages (Greene, 1988).

Some laboratory observations of the swimming behaviour of calanoid copepods are listed in Table I. It has been shown that a variety of (slow-swimming) patterns and postures are adopted by different species of calanoid copepods during swimming. Some species hang (or hover) almost at the same position in the water column (e.g. *Temora longicornis* and *Neocalanus cristatus*, both predominantly stationary suspension feeders) while generating a feeding current. Some other species are continuously cruising, like *Limnocalanus macrurus* and *Euchaeta elongata* that are raptorial predators. One species (*Clausocalanus furcatus*) swims very quickly with no evidence that it creates a feeding current. Between these two extremes, there are many species displaying an intermediate swimming behaviour, 'cruise and sink', or 'hop and sink', etc. Different species have different body orientations, ranging from vertical body orientation (with anterior pointing upwards or downwards) to horizontal body orientation, and some species can change their body orientation during swimming. The swimming direction can be upward, downward, backward, or forward, etc.

Laboratory observations have also shown that the properties of the flow field generated by a freely swimming copepod are closely related to the swimming behaviour of the copepod. Following are some examples. The flow field for the feeding mode of *Eucalanus crassus* was shown to be different from that for the cruising mode (Strickler, 1982), and the swimming behaviour for the feeding mode was actually different from that for the cruising mode. Six species of calanoid copepods with different swimming behaviours: (1) slow-moving or stationary suspension feeding (*Temora longicornis*, *Pseudocalanus elongatus* and *Paracalanus parvus*), (2) swimming fast interrupted by sinking periods (*Centropages typicus* and *Centropages hamatus*), or (3) motionless-sinking combined with short jumps (*Acartia clausi*) were shown to have different flow velocities and flow rates (Tiselius and Jonsson, 1990). Large differences in the geometry of flow fields were found between species, due to the differences in body orientation and trajectory of swimming behaviours (Bundy and Paffenhöfer, 1996).

No theoretical or numerical models are available to relate the flow field generated by a freely swimming copepod to the swimming motion of the copepod. In this and a companion paper (Jiang *et al.*, 2002), we develop such models. For this purpose, the Navier–Stokes equations governing the flow field generated by a freely swimming copepod will be simplified based on the characteristics of the beating movement of the copepod's cephalic appendages. The appendages provide propulsion for the copepod to swim in the water and contribute to the generation of a flow field around the copepod. Assuming steady motion, we will obtain the equations coupling the Navier–Stokes equations with the dynamic equations for the copepod's body. Then, the Stokes flow models that neglect inertia effects will be used to approximate the coupling equations and approximate solutions will be obtained in the case of highly simplified spherical geometry. Based on these solutions, the flow geometry and the velocity decay of the flow field for various swimming behaviours will be examined and compared. The present theoretical analysis is made possible by the strong simplifications of the real problem. More realistic Reynolds numbers and copepod geometries require the use of more complicated numerical techniques. An initial numerical study of the flow around a tethered copepod was described in Jiang *et al.* (Jiang *et al.*, 1999). A more general numerical study for the case of freely swimming copepods is described in the companion paper (Jiang *et al.*, 2002).

## THEORETICAL ANALYSIS

### Equations governing the three-dimensional flow field around a freely swimming copepod and forces on the copepod

Consider a freely swimming copepod in the water column and assume that the copepod generates a flow field around itself, that is to say, the fluid is otherwise quiescent in the absence of the copepod. The equations governing the velocity vector field $\mathbf{u}(\mathbf{x}, t)$ around the

*Table I: Swimming behaviour of calanoid copepods observed in laboratory*

| Species | Descriptions of the swimming behaviour |
|---|---|
| *Acartia clausi* female | Sank most of the time, interrupted by frequent jumps. The swift jumps, about three body lengths long, usually kept the copepod in the same vertical position. Occasionally while sinking, it made movements with its feeding appendages, which were quite different from suspension-feeding movements and apparently represented a raptorial behaviour when sensing individual objects. No suspension-feeding movements were observed. (Tiselius and Jonsson, 1990) |
| *Acartia tonsa* female | Behaviour 1: In low to moderately high food concentrations, *A. tonsa* mostly sank passively, often starting with a horizontal body orientation and a mean sinking velocity of 0.58 mm $s^{-1}$, and ending with a tendency to align along the vertical axis, reaching a terminal sinking velocity of 0.8 mm $s^{-1}$. About each second, *A. tonsa* darted upwards by a thrust of its antennules (and sometimes the thoracopods), lasting about 0.1 s.<br><br>Behaviour 2: In high food concentrations, *A. tonsa* devoted more than double the time to suspension feeding and did not reorient its body. (Jonsson and Tiselius, 1990) |
| *Centropages hamatus* female | Short time suspension feeding (0.4–0.6 s), followed by the long periods of sinking sometimes including apparent catching movements with the mouthparts. Vertical body orientation at the start of a feeding bout and then moved slowly in an arc or swam fast straight upwards (up to 7.2 mm $s^{-1}$). It sank with a horizontal orientation (1.4 mm $s^{-1}$) with its tail pointing upward. (Tiselius and Jonsson, 1990) |
| *Centropages typicus* female | After long suspension feeding bouts (1.9–4.0 s), the copepod sank for a long period with horizontal orientation (sinking velocity 1.0 mm $s^{-1}$), followed by upward swimming, 1.9 mm $s^{-1}$. (Tiselius and Jonsson, 1990) |
| *Centropages velificatus* female | Behaviour 1: These copepods followed curved paths as they swam upward for 3 to 6 s then, at the apex of each path, sank for 2 to 3 s at approximately 2 mm $s^{-1}$ to a vertical position close to the starting location. The copepods tilted backward while swimming and changed the body orientation gradually during each time series.<br><br>Behaviour 2: The copepod alternated long (3 to 12 s) bouts of linear swimming activity with short (0.5 to 1 s) sinking bouts. The copepod tilted forward while swimming and the body orientation remained relatively constant during each time series. At the end of each sinking bout, the copepod executed rapid turns by flicking either of its antennule. (Bundy and Paffenhöfer, 1996) |
| *Clausocalanus furcatus* female | Moved continuously along convoluted small loops at a mean speed of about 10 mm $s^{-1}$ (corresponding to 10 body lengths $s^{-1}$). This motion was occasionally interrupted by sudden somersaulting performed at very high speed (up to 17 mm $s^{-1}$). The copepods only occasionally sank (2 mm $s^{-1}$, which is very slowly). There was no evidence that *C. furcatus* created feeding currents. (Mazzocchi and Paffenhöfer, 1999) |
| *Diaptomus minutus* | Behaviour 1: Glided slowly (0.0–0.4 mm $s^{-1}$) by moving the feeding appendages, or either hung motionless in the water column or sank slowly, when not moving the feeding appendages. Interrupted by jumps of about one or two body lengths. (Wong *et al.*, 1986)<br><br>Behaviour 2: Swam backward while feeding on suspended algae for more than 2 s; the swimming speed is about 0.4 mm $s^{-1}$ and the beating movement of the feeding appendages can be seen from this observation. (J. R. Strickler, personal communication, 2000) |
| *Epischura lacustris* | Swam exclusively in the cruising mode (Strickler, 1982), i.e. spent most of the time either gliding slowly forwards along a smooth path or sinking passively through the water column, with a horizontal body orientation. Movements of the antennae provided most of the thrust during gliding, and no appendage movements during sinking. The copepod had the tendency to switch from one behaviour to another at much shorter intervals, and thus appeared to move in a jerky fashion. (Wong and Sprules, 1986) |
| *Eucalanus crassus* | All females swam backwards in a feeding bout at a speed of 1.75 mm $s^{-1}$ with the body axis vertical. After feeding bouts, sank passively, or ascended actively using the mouthparts, which has been termed the cruising mode. Males and copepodites swam, according to their sizes, at lower speeds. (Strickler, 1982) |
| *Euchaeta elongata* C4 female | Swam along a sinusoidal path, swimming slowly upwards against gravity, reorienting itself at the crest of its trajectory, and then swimming and gliding more rapidly downwards with gravity. (Greene and Landry, 1985) |

*Table I continued*

| Species | Descriptions of the swimming behaviour |
|---|---|
| *Euchaeta rimana* | Adult females exhibited a strong horizontal component to swimming at an average speed of 7.1 mm $s^{-1}$. The female copepod was oriented so that the paired setular array projecting from the antennules was pointed toward the swimming direction. Swimming was propelled by the beating of the antennae. If there was no appendage movement, the copepod immediately sank. The gentle cruising of the copepod was interrupted only briefly by the rapid turns which took less than 60 ms to execute. Adult males, which lack the setular array on their antennules, swam with a predominantly vertical component. The males swam up with their long axis of the body aligned with the flow at an average speed of 7.5 mm $s^{-1}$ and sank with their ventral surface down and urosome arched at an average speed of 5.0 mm $s^{-1}$. Upward swimming was accomplished by the beating of the antennae. No motion of the mouthparts or swimming legs occurred during sinking. (Yen, 1988) |
| *Limnocalanus macrurus* | Glided slowly forwards with a horizontal body orientation, broken periodically by rapid jumps. The jumps typically covered distances of only one to two body lengths, and were distinctly different from escape jumps. Never stopped swimming, and thus did not sink or hang motionless in the water. (Wong and Sprules, 1986) |
| *Macrosetella gracilis* | Swam primarily with a jerky forward motion. When not swimming forward, the copepod usually appeared to be using its anterior ventral appendages to grasp particles. Forward jumps rarely measured one body length. (Hwang and Turner, 1995) |
| *Metridia pacifica* female | Swam continuously in a smooth glide with sharp change in direction from time to time. Swimming direction was predominantly horizontal, and a horizontal body orientation was maintained all the time. (Wong, 1988b) |
| *Neocalanus cristatus* C5 | This large copepod (total length 7.1–8.9 mm) was an infrequent swimmer, typically spending greater than 90% of its time hanging motionless in the water column. It was capable of producing a powerful feeding current with or without subsequent translational motion of the body. Food was entrained by this current and bought into the capture area. (Greene and Landry, 1988) |
| *Paracalanus aculeatus* female | These copepods swam in linear paths and rarely exhibited periodic sinking. The copepod tilted forward while swimming, and the body orientations of the copepods were relatively constant during each time series. The copepods changed direction in the horizontal plane by flicking an antennule and turning rapidly. They also occasionally ceased appendage movement and sank at approximately 2 mm $s^{-1}$. (Bundy and Paffenhöfer, 1996) |
| *Paracalanus parvus* female | Moved upward in an arc during short feeding bouts (1.2–2.0 s) at a swimming speed of 0.6 mm $s^{-1}$ and subsequently sank with the same velocity. Body orientation was nearly vertical both when swimming and sinking. (Tiselius and Jonsson, 1990) |
| *Pseudocalanus elongatus* female | Moved mainly horizontally or rose slowly during long feeding bouts (lasting 9 to 18 s each), swimming velocity 0.5 mm $s^{-1}$. When not suspension feeding, sank at 1.1 mm $s^{-1}$. Body orientation was always constant with feeding appendages pointing obliquely upwards. (Tiselius and Jonsson, 1990) |
| *Pseudocalanus minutus* | Most of the time alternated between swimming, when they glided smoothly using the mouthparts, and pausing, when they sank with its caudal-end first. Both swimming and sinking were occasionally interrupted by short jumps of about one or two body lengths. However, jumps were extremely rare and occupied a very small portion of the animal's time. (Wong, 1988a) |
| *Senecella calanoides* | Most of the time they either glided slowly backwards along a smooth path or sank passively through the water column, with a vertical body orientation. Movements of the antennae provided most of the thrust during gliding, and there was no appendage movement during sinking. (Wong and Sprules, 1986) |
| *Temora longicornis* female | Continuous suspension feeding, never observed sinking. Virtually immobile while performing long feeding bouts (8.7–9.0 s). No loops and only very small corrections of body orientation were observed. In suspension feeding the individual remained vertically oriented and slowly drifted horizontally or slightly upward. (Tiselius and Jonsson, 1990) |
| *Temora turbinata* | Glided smoothly and continuously either straight ahead in curving arcs or in circles. In most cases, this swimming was accomplished by the ventral anterior feeding appendages (the antennae, maxillules, maxillae and maxillipeds) while creating a feeding current. (Hwang and Turner, 1995) |
| *Undinula vulgaris* var. *taiwanicus* | Primarily swam forwards by creating a feeding current, punctuated by motionless periods of equal or greater length than periods of motion. Spent most of the time in the vertical plane with its head pointing toward the surface of the water. Moved upward when swimming, and sank when at rest, the typical hop and sinking swimming pattern. (Hwang and Turner, 1995) |

copepod are the Navier–Stokes equations and the continuity equation:

$$\rho \frac{\partial \mathbf{u}}{\partial t} + \rho \mathbf{u} \cdot \nabla \mathbf{u} = -\nabla p + \mu \nabla^2 \mathbf{u} \quad (1)$$

$$\nabla \cdot \mathbf{u} = 0 \quad (2)$$

where $\rho$ is the density of the fluid (about $1.030 \times 10^3$ kg $m^{-3}$ for sea water), $\mu$ is the dynamic viscosity (about $1.390 \times 10^{-3}$ kg $m^{-1}$ $s^{-1}$ for sea water) and $p$ is the flow pressure field. The density of the fluid is assumed to be uniform, and hence gravity is not considered since it only contributes to a hydrostatic pressure and has no effect on the flow field. The boundary conditions of equations (1) and (2) are no relative velocity at the body surface and zero velocity at infinity.

On the other hand, the motion of the copepod is governed by the equations derived from Newton's second law, which relates the forces (as well as the associated torques) acting on the copepod's body to its acceleration. The forces include the forces exerted by the flow on the copepod due to the distributions of flow pressure and shear stress around the surface of the copepod, the buoyancy force and the body force due to gravity [see Figure 1 and Table I in (Jiang *et al.*, 1999)].

The boundary conditions on the body–fluid interface (including the surface of the cephalic appendages) couple the equations governing the flow field around the copepod with those controlling the motion of the copepod. Table I suggests that the slow-swimming pattern and body posture of copepods are related to the high-frequency beating movement of the cephalic appendages. By controlling the beating movement, the body orientation and the abdomen posture, i.e. by controlling the boundary condition on the body–fluid interface, a freely swimming copepod is able to control the flow field around itself and hence the forces exerted by the water flow on its body.

Since a freely swimming copepod may perform a complex swimming pattern by moving at a translation velocity while rotating its body to change the swimming direction, it is difficult to deal with the boundary condition on the body–fluid interface. Moreover, the high-frequency beating of the cephalic appendages further complicates the boundary condition on the surface of these appendages. Analytical solutions for the coupling equations are impossible to determine under such complex conditions. Simplifications have to be made in order to make the problem solvable. In the following two subsections, we will first examine the characteristics of the beating movement of the cephalic appendages that provide propulsion and contribute to the generation of the flow field around a copepod's body. Then, equation (1) will be simplified based on these characteristics, and the simplified coupling equations will be derived for a copepod in steady motion.

## Generation of feeding current and propulsion

Many calanoid copepods use their cephalic appendages to propel themselves smoothly through the water column. In addition to providing propulsion, the beating movement of the cephalic appendages, in most cases, also generates a quasi-steady feeding current that benefits the feeding of copepods. Generally, two characteristics are common in calanoid copepods that use the beating movement to generate a quasi-steady feeding current as well as propulsion.

One of the characteristics is that the beating movement is rapid, i.e. the beating movement occurs at a high frequency. This kind of motion pattern of the cephalic appendages in calanoid copepods has been observed for a long time (Storch and Pfisterer, 1925; Cannon, 1928; Lowndes, 1935; Koehl and Strickler, 1981) and recorded for a number of copepod species by several researchers (Price *et al.*, 1983; Price and Paffenhöfer, 1986a,1986b; Gill, 1987). As shown in Figure 3 of Gill (Gill, 1987), different species elicit different beating frequencies and patterns. The antennae of some species, such as *Temora longicornis*, *Isias claviceps*, *Pseudocalanus elongatus* and *Centropages hamatus*, perform a high-frequency beating movement; those species have also been observed to generate a feeding current and glide smoothly in the water column (see Table I). While the beating frequency of the antennae of some other species [e.g. *Anomalocera patersoni* and *Acartia clausi*, as also shown in Figure 3 of (Gill, 1987)] is quite low; neither species generates a feeding current and they both swim in a jerky fashion (Gauld, 1966; Jonsson and Tiselius, 1990).

The other characteristic is that the cephalic appendages usually operate in specific motion patterns during swimming and feeding. Gauld (Gauld, 1966) probably noticed this characteristic first. It has been pointed out that for many genera of calanoid copepods (such as *Calanus*, *Pseudocalanus*, *Euchaeta*, *Centropages*, *Isias*, *Temora*, *Diaptomus* and *Eurytemora*, which glide smoothly through the water column and generate a quasi-steady feeding current), their antennae, mandibles and maxillules are bi-ramous including an endopod and an exopod [see Figure 3a in (Gauld, 1966)]. During swimming slowly, the appendages perform a double-acting stroke in which the endopods and exopods of the appendages beat alternately [see Figure 1 in (Gauld, 1966)]. Here, the copepod spreads out the setae equipped on the surface of its endopod or exopod to exert the maximum thrust on the water during a propulsive stroke and holds the setae to reduce its drag during a recovery stroke. The alternate beating of the endopods and exopods and the asymmetry in the propulsive stroke

and the recovery stroke are very important in generating nearly continuous propulsion for copepods to swim slowly in the water column.

This characteristic has also been noticed by Strickler (Strickler, 1984), who proposed a mechanism to understand the generation of the feeding currents by calanoid copepods after a detailed observation of the movement of the cephalic appendages of a tethered *Eucalanus pileatus* by using high-speed microcinematography. There are two pairs of appendages performing the 'fling and clap' motion pattern. The maxilliped and the endopod of the second antenna form the larger pair [see Figure 2a in (Strickler, 1984)]; the exopod of the maxillule and of the second antenna form the smaller pair [see Figure 2b in (Strickler, 1984)]. The copepod flaps the two pairs of appendages (at each side of the body) like a butterfly flapping its wings. It has also been shown that the mandibular palp executes a three-dimensional movement that governs the direction of the flow and that there is no motion of the maxilla [see Figure 2c in (Strickler, 1984)]. In addition, these movements are carried out with high precision by the appendages and there exists a clear timing pattern [see Figure 3 in (Strickler, 1984); see also Figure 3 in (Price and Paffenhöfer, 1986b)]. The above-described motion pattern generates the feeding current and enables the copepod precisely to direct and handle the approaching food particles in the current.

Concerning the generation of propulsion, the film was re-examined by courtesy of Prof. J. Rudi Strickler. The mandibular palp was clearly shown to perform an asymmetric pattern of motion, i.e. the whole appendage is stretched out and the setae on its surface spread out during a propulsive stroke, and the appendage lowers its limb and holds the setae during a recovery stroke. Asymmetry is also displayed by the appendages performing the 'fling and clap' motion pattern. The asymmetry together with the timing pattern leads to the generation of propulsion. However, the evidence has only been collected for tethered copepods; no detailed observation has been made of the motion pattern of the cephalic appendages of a freely swimming copepod. We do not know whether the copepod changes its motion pattern when switching from hovering to swimming or from swimming slowly to swimming quickly. How the motion pattern of the cephalic appendages relates to the complex swimming and feeding behaviours remains an important unanswered question.

## Simplifications of the Navier–Stokes equations

*Steady flow and force field*

It is complicated to deal with the unsteady Navier–Stokes equations with time-dependent moving boundary conditions. However, we are only interested in the flow field at the scale of a copepod's body length and at a time scale much longer than the time scale of the beating movement of the cephalic appendages. On the grounds of dimensional analyses described below and taking into account the two characteristics of the beating movement of the cephalic appendages (see above), we can simplify the problem by removing the unsteady terms governing the flow field in the vicinity of the moving (oscillating) appendages and by replacing the effects of the time-dependent moving boundary conditions at the surface of the beating appendages with a forcing term added to the right-hand side of the Navier–Stokes equations.

Generally, the diameter of the cephalic appendages ($d$) of calanoid copepods ranges from 20 μm to 200 μm as seen from the figures in Huys and Boxshall (Huys and Boxshall, 1991), so that reasonably we can choose $d = 100$ μm as representative value. According to Figure 3 in Gill (Gill, 1987), the beating frequency of appendages is then chosen as $f = 20$ Hz, and $\omega = 2\pi f$. With these parameters and $\nu = \mu/\rho = 1.350 \times 10^{-6}$ m$^2$ s$^{-1}$, it turns out that the viscous length scale

$$\delta = \sqrt{\frac{2\nu}{\omega}} \approx 147\mu\text{m} \qquad (3)$$

is of the same order of magnitude as the diameter of the cephalic appendages. This indicates that the flow field is unsteady within the distance of $\delta$ away from the surface of the appendages, but that the unsteadiness can be neglected at distance much larger than $\delta$ [(Landau and Lifshitz, 1959); see also (Panton, 1996)]. Thus, if we only pay attention to the flow field around a copepod at the scale of the copepod's body length, the flow field can be considered to be quasi-steady. Only the non-zero mean of the flow field resulting from the asymmetrical motion pattern (and probably also from the timing pattern) can be seen at the scale of the copepod's body length. In addition, the time scale of the feeding current is much longer than the time scale of the beating movement of the cephalic appendages. Many observations have revealed that already at a short distance away from the beating appendages, the flow field around a feeding copepod is quasi-steady.

We choose to separate the appendages that perform the beating movement from the main body (denoted as $\Omega_{mb}$) of the copepod. Hence the surface force exerted by the water on these appendages can be separated from the forces acting on the surface of the main body. The mean effect of the beating movement of these appendages may be taken as a set of distributed forces exerted (by the appendages) on the water at the positions where the appendages are located. [Note that the distributed forces include the thrust (propulsion) originated from both the drag on these

appendages and the fluid acceleration.] On the other hand, according to Newton's third law, the adjacent water exerts equal and opposite forces on these appendages. Application of Newton's second law and third law shows that the appendages exert a force on the body equal to the force exerted by the water on the appendages. The separation enables us to avoid the moving boundary condition that is difficult to incorporate into theoretical analyses as well as numerical simulations. However, the main body of the copepod remains in the model, and a no-slip boundary condition is satisfied on its surface.

Thus, the governing equations for the quasi-steady flow field around a copepod can be written as:

$$\rho\mathbf{u}\cdot\nabla\mathbf{u} = -\nabla p + \mu\nabla^2\mathbf{u} + \mathbf{f}_a \tag{4}$$

$$\nabla\cdot\mathbf{u} = 0 \tag{5}$$

with the no-slip boundary condition on the surface of the main body, $\Omega_{mb}$:

$$\mathbf{u} = \mathbf{V}_{swimming}, \text{ at } \Omega_{mb} \tag{6}$$

and the boundary condition at infinity:

$$\mathbf{u} \to 0, \text{ at infinity} \tag{7}$$

Here, $\mathbf{V}_{swimming}$ is the swimming velocity of the copepod. In equation (4), $\mathbf{f}_a$ represents the force field (force per unit volume) that models the effect of the beating movement of the cephalic appendages. Since the appendages are spatially distributed (ventrally to the copepod), $\mathbf{f}_a(\mathbf{x})$ is interpreted as a distributed force field. If the copepod is assumed in a steady motion, i.e. either hovering at a same position ($\mathbf{V}_{swimming} = 0$) or swimming at a constant velocity ($\mathbf{V}_{swimming}$ = constant), the integral of $\mathbf{f}_a(\mathbf{x})$ can be evaluated from the force-balance of the copepod's body:

$$\mathbf{W}_{excess} + \mathbf{F} - \int_{\mathbf{x}} \mathbf{f}_a(\mathbf{x})\, d\mathbf{x} = 0 \tag{8}$$

where $\mathbf{W}_{excess}$ is the excess weight of the copepod, and $\mathbf{F}$ is the drag force exerted by the flow field on the copepod's main body. Equations (4) to (8) are actually the desired coupling equations between the steady Navier–Stokes equations and the dynamic equations for the body of a copepod in steady motion.

*Linearization of the equations*

We nondimensionalize equation (4) by scaling distance by the body length $L$, $\mathbf{u}$ by some characteristic velocity $U$, and pressure by $\mu U/L$. Substituting the nondimensional variables (denoted by primes) $\mathbf{x}' = \mathbf{x}/L$, $\mathbf{u}' = \mathbf{u}/U$, and $p' = p/(\mu U/L)$, equation (4) becomes

$$Re\ \mathbf{u}'\cdot\nabla'\mathbf{u}' = -\nabla' p' + \nabla'^2\mathbf{u}' + \frac{L^2}{\mu U}\mathbf{f}_a \tag{9}$$

The dimensionless number $Re$ is the Reynolds number $Re = \rho UL/\mu$. It represents the magnitude of inertial convective forces relative to viscous forces. When $Re<<1$, the nonlinear term on the left-hand side of equation (9) is small compared with those on the right-hand side and thus may be neglected. This is often also called the inertia-free approximation. Usually, the Reynolds number of the flow field around a real copepod does not satisfy the condition of $Re<<1$, and is instead of the order $Re\sim1$. However, especially in the near field, we may still gain important insights into the flow properties by considering the inertia-free approximation and thus allow analytical solutions to the simplified problem. Reverting to dimensional variables, the linearized form of equation (9) that will be solved below is written as

$$-\nabla p + \mu\nabla^2\mathbf{u} + \mathbf{f}_a = 0 \tag{10}$$

which is the Stokes equation.

*Geometry simplification*

In order to obtain analytical solutions, a further simplification, namely of the geometry of copepods, is needed. In the present study, a spherical body shape is assumed for a model copepod. In the following section, we will first review some basic solutions of Stokes flow, then the detailed description of the spherical model copepod will be given and classical analytical solutions of the flow field around a sphere will be applied to describe the different steady motions of the spherical model copepod.

It is stressed that the simplification of the geometry and the linearization of the Navier–Stokes equations are performed only to allow analytical solutions of the flow field to be obtained. To account for additional effects of finite $Re$ (i.e. including inertia effects) and for more realistic body shapes, equations (4) to (8) are solved numerically in Jiang *et al.* (Jiang *et al.*, 2002).

## STOKES FLOW MODELS OF FIVE STEADY MOTION MODES OF A SPHERICAL COPEPOD

### Some basic solutions of Stokes flow

*Green's functions of Stokes flow*

The solutions of equations (10) and (5) can be derived through the method of Green's functions. [after (Pozrikidis, 1992)]. The Green's functions of Stokes flow

represent solutions of the continuity equation (5) and the singularly forced Stokes equation

$$-\nabla p + \mu\nabla^2 \mathbf{u} + \mathbf{f}\,\delta(\mathbf{x}-\mathbf{x}_0) = 0 \tag{11}$$

where $\mathbf{f}$ is an arbitrary constant, $\mathbf{x}_0$ is an arbitrary point, and $\delta$ is the three-dimensional delta-Dirac function. If we adopt the indicial notations (with the *xyz* axis referred to as $x_i$, $i$ = 1, 2, 3), the solution of equation (11) can be written in terms of the Green's function $\mathbf{G}$ as

$$u_i(\mathbf{x}) = \frac{1}{8\pi\mu} G_{ij}(\mathbf{x},\mathbf{x}_0) f_j \tag{12}$$

where $\mathbf{x}_0$ is the pole or the source point, and $\mathbf{x}$ is the observation or field point. Physically, equation (12) expresses the velocity field due to a concentrated point force of strength $\mathbf{f}$ placed at the point $\mathbf{x}_0$. The Green's function $\mathbf{G}$ depends on the boundary geometry of the flow. In the present study, we are interested in two Green's functions. The first one is the free-space Green's function (denoted by $\mathbf{G}^{\mathrm{FREE}}$) for infinite unbounded flow, also called the Stokeslet, or the Oseen–Burgers tensor, and written as (Pozrikidis, 1992)

$$G_{ij}^{\mathrm{FREE}}(\hat{\mathbf{x}}) = \frac{\delta_{ij}}{r} + \frac{\hat{x}_i \hat{x}_j}{r^3} \tag{13}$$

where $r = |\hat{\mathbf{x}}|, \hat{\mathbf{x}} = \mathbf{x} - \mathbf{x}_0$.

The second one is the Green's function $\mathbf{G}^{\mathrm{SPH}}$ obtained by Oseen in 1927 for an infinite flow bounded internally by a solid sphere [(Pozrikidis, 1992); see also (Higdon, 1979)]. The result is

$$G_{ij}^{\mathrm{SPH}}(\mathbf{x},\mathbf{x}_0) = \left(\frac{\delta_{ij}}{r} + \frac{\hat{x}_i \hat{x}_j}{r^3}\right) - \frac{a}{|\mathbf{x}_0|}\frac{\delta_{ij}}{r^*} - \frac{a^3}{|\mathbf{x}_0|^3}\frac{\hat{x}_i^* \hat{x}_j^*}{(r^*)^3}$$
$$-\frac{|\mathbf{x}_0|^2 - a^2}{|\mathbf{x}_0|}\left[\frac{X_i^* X_j^*}{a^3 r^*} - \frac{a}{|\mathbf{x}_0|^2 (r^*)^3}\left(X_i^* \hat{x}_j^* + X_j^* \hat{x}_i^*\right)\right. \tag{14}$$
$$\left. + \frac{2X_i^* X_j^*}{a^3}\frac{X_k^* \hat{x}_k^*}{(r^*)^3}\right] - \frac{\left(|\mathbf{x}|^2 - a^2\right)\left(|\mathbf{x}_0|^2 - a^2\right)}{2|\mathbf{x}_0|^3}\frac{\partial \phi_j}{\partial x_i}$$

with

$$\frac{\partial \phi_j}{\partial x_i} = -\frac{3X_j \hat{x}_i^*}{a(r^*)^3} + \frac{a\delta_{ij}}{(r^*)^3} - \frac{3a\hat{x}_i^* \hat{x}_j^*}{(r^*)^5} - \frac{2X_j X_i^*}{a(r^*)^3} + \frac{6X_j \hat{x}_i^* \hat{x}_k^* X_k^*}{a(r^*)^5}$$
$$+\frac{3a}{|\mathbf{X}^*|}\frac{X_j^* \hat{x}_i^* (r^*)^2 + \hat{x}_i^* \hat{x}_j^* |\mathbf{X}^*|^2 + \left(r^* - |\mathbf{X}^*|\right)(r^*)^2 |\mathbf{X}^*| \delta_{ij}}{(r^*)^3 |\mathbf{X}^*|\left(|\mathbf{X}^*| r^* + x_k X_k^* - |\mathbf{X}^*|^2\right)}$$
$$-\frac{3a}{|\mathbf{X}^*|}\frac{\left(|\mathbf{X}^*| \hat{x}_i^* + r^* X_i^*\right)\left[X_j^* (r^*)^2 - \hat{x}_j^* |\mathbf{X}^*|^2 + \left(\hat{x}_j^* - X_j^*\right) r^* |\mathbf{X}^*|\right]}{(r^*)^2 |\mathbf{X}^*|\left(|\mathbf{X}^*| r^* + x_k X_k^* - |\mathbf{X}^*|^2\right)^2} \tag{15}$$
$$-\frac{3a}{|\mathbf{X}^*|}\frac{x_i X_j^* + |\mathbf{x}||\mathbf{X}^*|\delta_{ij}}{|\mathbf{x}|\left(|\mathbf{x}||\mathbf{X}^*| + x_k X_k^*\right)} + \frac{3a}{|\mathbf{X}^*|}\frac{\left(|\mathbf{X}^*| x_i + |\mathbf{x}| X_i^*\right)\left(|\mathbf{X}^*| x_j + |\mathbf{x}| X_j^*\right)}{|\mathbf{x}||\mathbf{X}^*|\left(|\mathbf{x}||\mathbf{X}^*| + x_k X_k^*\right)^2}$$

Here $a$ is the radius of the sphere and

$$\hat{\mathbf{x}} = \mathbf{x} - \mathbf{x}_0, \qquad r = |\hat{\mathbf{x}}|,$$
$$\mathbf{X}^* = \frac{a^2}{|\mathbf{x}_0|^2}\mathbf{x}_0, \qquad \hat{\mathbf{x}}^* = \mathbf{x} - \mathbf{X}^*, \qquad r^* = |\hat{\mathbf{x}}^*| \tag{16}$$

Note that the point force is located at $\mathbf{x}_0$. For convenience, it has been assumed that the centre of the sphere is the origin of the coordinate system.

For later references, the drag force acting on the solid sphere due to the flow produced by the point force $\mathbf{f}$ is given by

$$\mathbf{F} = \frac{1}{2}\left(\frac{3a}{r} - \frac{a^3}{r^3}\right)\mathbf{f}_r + \frac{1}{4}\left(\frac{3a}{r} + \frac{a^3}{r^3}\right)\mathbf{f}_t \tag{17}$$

where $\mathbf{f}_r = \mathbf{e}_r(\mathbf{f}.\,\mathbf{e}_r)$ is the radial component of $\mathbf{f}$, $\mathbf{e}_r$ is the unit vector in the radial direction emanating from the centre of the sphere, and $\mathbf{f}_t = \mathbf{f} - \mathbf{e}_r(\mathbf{f}.\,\mathbf{e}_r)$ is the transverse component of $\mathbf{f}$ (Pozrikidis, 1992).

*Stokes flow due to the translating motion of a solid sphere*

The Stokes flow field produced by a solid sphere of radius $a$ translating with velocity $\mathbf{U}$ in an ambient fluid of infinite expanse is

$$u_i(\mathbf{x}) = \frac{1}{4}\frac{a}{r}\left(3 + \frac{a^2}{r^2}\right)U_i + \frac{3}{4}\frac{a}{r}\left(1 - \frac{a^2}{r^2}\right)\frac{x_i' x_j'}{r^2}U_j \tag{18}$$

in a stationary frame of reference. It satisfies the boundary condition $\mathbf{u} = \mathbf{U}$ at $r = a$ (Pozrikidis, 1997). Here, $r = |\mathbf{x}'|, \mathbf{x}' = \mathbf{x} - \mathbf{x}_c$, $\mathbf{x}_c$ is the centre of the sphere. If the frame of reference is fixed on the sphere, the expression for the velocity field is

$$u_i(\mathbf{x}) = -U_i + \frac{1}{4}\frac{a}{r}\left(3 + \frac{a^2}{r^2}\right)U_i + \frac{3}{4}\frac{a}{r}\left(1 - \frac{a^2}{r^2}\right)\frac{x_i x_j}{r^2}U_j \tag{19}$$

For convenience, the centre of the sphere is chosen to be the origin of the frame of reference, and $r = |\mathbf{x}|$.

Correspondingly, equation (19) satisfies the boundary condition $\mathbf{u} = 0$ at $r = a$.

The drag force on the sphere by the flow is obtained through the celebrated Stokes' law:

$$\mathbf{F} = -6\pi\mu a\mathbf{U} \tag{20}$$

*Linear combination of Stokes solutions*

The linearity of equation (10) allows the use of linear combinations of solutions to obtain new solutions of the equation. Consider the Stokes flow generated by a solid sphere of radius $a$ with a point force $\mathbf{f}$ outside the sphere. The whole system, including the solid sphere and the point force, translates with velocity $\mathbf{U}$ through the fluid otherwise at rest (the point force is motionless relative to the sphere). The velocity field generated by this translating system can be derived through a linear combination of equations (12) and (19) [or (18)].

In a frame of reference fixed on the sphere and by choosing the centre of the sphere as the origin of the frame of reference, the solution for the velocity field can be written as

$$u_i(\mathbf{x}) = -U_i + \frac{1}{4}\frac{a}{r'}\left(3 + \frac{a^2}{r'^2}\right)U_i + \frac{3}{4}\frac{a}{r'}\left(1 - \frac{a^2}{r'^2}\right)\frac{x_i x_j}{r'^2}U_j + \frac{1}{8\pi\mu}G_{ij}^{\mathrm{SPH}}(\mathbf{x}, \mathbf{x}_0)\, f_j \tag{21}$$

where $r' = |\mathbf{x}|$, and the Green's function $\mathbf{G}^{\mathrm{SPH}}$ is calculated according to equations (14), (15) and (16). Equation (21) satisfies the boundary condition $\mathbf{u} = 0$ at $r = a$. Also, the solution can be written in a stationary frame of reference by transforming the velocity appropriately. Moreover, the drag force on the solid sphere by the flow described by equation (21) can be calculated through linear combination (addition) of equations (17) and (20).

## Five Stokes flow models for a spherical copepod in steady motion

Figure 1 shows schematically a spherical copepod for which Stokes flow models can be used to calculate analytically the flow field around the copepod's body under some steady motion modes. The radius $a$ of the spherical copepod is set to be 0.5 mm. The effect of the beating movement of the cephalic appendages is represented by a point force $\mathbf{f}$ outside the spherical body. For convenience, the positive $z$-direction is opposite to the direction of gravity, the pole of the point force is chosen on the positive $x$-axis, and the distance from

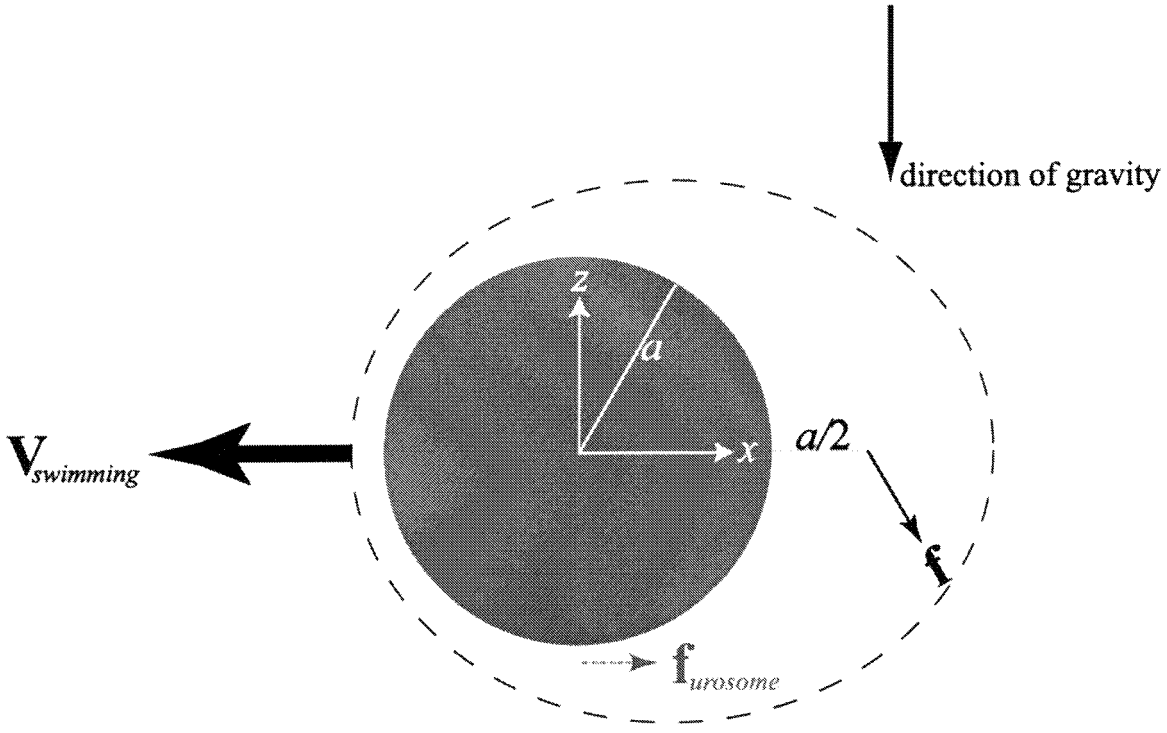


**Fig. 1.** Schematic illustration of the model copepod consisting of a spherical body of radius $a$ and a point force $\mathbf{f}$ (representing the effects of the cephalic appendages) located outside the spherical body at a distance of $a/2$ away from the surface of the spherical body. The positive $z$-direction is opposite to the direction of gravity. The point force $\mathbf{f}$ is placed on the positive $x$-axis. The whole system translates at a constant velocity $\mathbf{V}_{swimming}$ through the water. $\mathbf{f}_{urosome}$ represents the effects of the beating of the urosome, however it is neglected in the present work. (Note that this is not a free body diagram.)

the pole to the surface of the sphere is $a/2$. (For later references, $\mathbf{i}$ and $\mathbf{k}$ denote the unit vectors in the $x$- and $z$-directions, respectively.) $\mathbf{V}_{swimming}$ is the swimming velocity of the copepod and is a prescribed constant for steady motion.

A freely swimming copepod is a self-propelled body moving through the water. The thrust force (or propulsion) that a copepod derives from the reaction (and probably also from the drag) of the surrounding water by beating its cephalic appendages during steady swimming (i.e. at a constant mean velocity) must balance the resistive drag force (on its main body) and the excess weight of its body. Thus, we can understand the above-described model copepod in the following way. On one hand, the spherical copepod uses its appendages to apply a point force $\mathbf{f}$ to the water at a location outside its body. According to Newton's third law, simultaneously the copepod's body receives a reaction force $-\mathbf{f}$ from the water (which is equal to the reaction force of the water on the appendages, transmitted to the body). On the side of the surrounding water, the translating motion of the spherical body and the point force $\mathbf{f}$ together generate the water flow around the copepod. At the same time, this water flow exerts a drag force $\mathbf{F}$ on the copepod's body. When the copepod is in steady motion, the force–balance equation of the spherical copepod is written as

$$\mathbf{W}_{excess} + \mathbf{F} - \mathbf{f} = 0 \tag{22}$$

where $\mathbf{W}_{excess}$ is the excess weight of the copepod. Since the drag force $\mathbf{F}$ is a function of both $\mathbf{V}_{swimming}$ and the point force $\mathbf{f}$, and can be formulated as a linear combination of equations (17) and (20), the point force $\mathbf{f}$ (magnitude and direction) can be generally determined from equation (22) for various modes of steady motion. After the point force $\mathbf{f}$ is known, the flow field around the copepod is determined.

It is worth noting that (some) copepods can beat their urosome to apply additional forces to the surrounding water and the applied forces contribute to the torque balance of the copepods' body (Strickler, 1982). However, the forces due to the urosome beating are small relative to the forces applied by the beating cephalic appendages and contribute little to the flow field, and are therefore neglected in the present study. [Owing to its complexity, we cannot deal with the balance of torques on a copepod and simply assume that choosing a suitable centre of mass relative to the centre of volume enforces the torque balance. Note that in most situations the centre of mass is not identical to the centre of volume (Strickler, 1982).]

In the following subsections, five modes of steady motion will be considered: hovering, sinking freely, swimming upwards, swimming backwards, and swimming forwards. Based on the swimming behavioirs listed in Table I, it is reasonable to take these five motion modes as the idealized fashions in which a spherical copepod can swim, in real water. 'Idealized' means different from Nature but not too far from the truth, and the underlying physics is the same. However, we have to admit that a real copepod can only have certain swimming behaviours, and that we allow the model copepod to have so many swimming behaviours only for the purpose of comparison.

Prescribing the excess weight of the spherical model copepod is a subtle choice. Since the body volume of the spherical model copepod is several times larger than that of a real copepod with the same body length, it is preferable to calculate the excess weight according to the body volume of a real copepod. In this way, we match the magnitudes of velocity field to those associated with a real copepod with the same body length, since the magnitudes of the velocity field are dependent to a great extent on the magnitude of excess weight. According to Yen *et al.* (Yen *et al.*, 1998), the body volume of a copepod can be roughly calculated as

$$\Omega_{copepod} = \pi R^2 L \tag{23}$$

where $R = 0.25$ mm is the half body width, and $L = 1.0$ mm is the body length. Then, the excess weight is calculated according to the formula

$$\mathbf{W}_{excess} = \Delta\rho\Omega_{copepod}\mathbf{g} \tag{24}$$

where $\Delta\rho$ is the copepod's excess density relative to sea water, and $\mathbf{g}$ is the acceleration due to gravity. By choosing an excess density of 30 kg m$^{-3}$ [(Tiselius and Jonsson, 1990); for the body weight and volume of copepod species, see (Mauchline, 1998)], we obtain $\mathbf{W}_{excess} = -5.77 \times 10^{-8}\mathbf{k}$ N (the negative sign is because of the setting of the vertical ($z$-) axis in the coordinate system, and $\mathbf{k}$ is the unit vector in the z-direction). This is the value assigned to the excess weight of the spherical model copepod.

*Hovering model*

When the model copepod hovers (like a helicopter) in the water column, i.e. the swimming velocity $\mathbf{V}_{swimming} = 0$, the drag force on the copepod is only due to the flow generated by the point force $\mathbf{f}$ (Figures 2a and 2b). Also, it can be seen that the point force $\mathbf{f}$ has to be applied in the direction of gravity (negative $z$-direction), so that from equation (17) one can obtain the drag force

$$\mathbf{F} = \frac{1}{4}\left(\frac{3}{\beta} + \frac{1}{\beta^3}\right)\mathbf{f} \tag{25}$$

where $\beta=(a+a/2)/a=1.5$. Then, from the force–balance equation (22), one can easily obtain the point force

$$\mathbf{f} = \frac{\mathbf{W}_{excess}}{1 - \frac{1}{4}\left(\frac{3}{\beta} + \frac{1}{\beta^3}\right)} = 2.348 \cdot \mathbf{W}_{excess} \quad (26)$$

For the excess weight $\mathbf{W}_{excess} = -5.77 \times 10^{-8}\mathbf{k}$ N, the point force $\mathbf{f}$ is $-1.355 \times 10^{-7}\mathbf{k}$ N.

*Freely sinking model*

When the model copepod stops beating its cephalic appendages, so that the point force $\mathbf{f} = 0$, it sinks freely due to gravity (Figures 2c and 2d). In the final steady state, the drag force resulting from sinking balances the excess weight. The terminal velocity of sinking can be easily found as

$$\mathbf{V}_{terminal} = \frac{\mathbf{W}_{excess}}{6\pi\mu a} \quad (27)$$

For $\mathbf{W}_{excess} = -5.77 \times 10^{-8}\mathbf{k}$ N, the terminal velocity $\mathbf{V}_{terminal}$ is about $-4.4\,\mathbf{k}$ mm s$^{-1}$.

In the other examples below, we consider swimming model-copepods. In order to examine the effect of the swimming velocity, two cases will be considered in each configuration: swimming at a speed that is one-quarter of the terminal velocity, and equal to the terminal velocity.

*Upward swimming model*

When the model copepod swims upward (positive $z$-direction) with velocity $V_{swimming}\mathbf{k}$, where $V_{swimming} = |\mathbf{V}_{swimming}|$, the drag force on the copepod has to be calculated through linear combination of equations (17) and (20). Then, simple algebra of the force–balance equation (22) yields

$$\mathbf{f} = \frac{-6\pi\mu a V_{swimming}\mathbf{k} - W_{excess}\mathbf{k}}{1 - \frac{1}{4}\left(\frac{3}{\beta} + \frac{1}{\beta^3}\right)} \quad (28)$$

where $W_{excess} = |\mathbf{W}_{excess}|$ and $\beta = (a + a/2)/a = 1.5$. The direction of the point force $\mathbf{f}$ is still in the direction of gravity (negative $z$-direction).

The free body diagram of this model is drawn in Figures 2e and 2f. It is quite similar to the hovering model. However, the magnitude of the point force $\mathbf{f}$ (also the magnitude of the drag force $\mathbf{F}$) is larger than the hovering model due to the additional upward translating motion. For example, for the excess weight $\mathbf{W}_{excess} = -5.77 \times 10^{-8}\mathbf{k}$ N, if $\mathbf{V}_{swimming} = 1.1\,\mathbf{k}$ mm s$^{-1}$ (one-quarter of the terminal velocity), $\mathbf{f} = -1.693 \times 10^{-7}\mathbf{k}$ N, and if $\mathbf{V}_{swimming} = 4.4\,\mathbf{k}$ mm s$^{-1}$ (the terminal velocity), $\mathbf{f} = -2.708 \times 10^{-7}\mathbf{k}$ N. The magnitudes for both are larger than for the hovering model.

*Backward swimming model*

When the model copepod swims horizontally backward ~~is the unit vector in the $x$-direction~~ (negative $x$-direction) with velocity $-V_{swimming}\mathbf{i}$, ($\mathbf{i}$ is the unit vector in the $x$-direction), the point force $\mathbf{f}$ is no longer applied in the direction of gravity (negative $z$-direction). While the copepod pushes water downward to overcome the excess weight, it has to simultaneously push water forwards in order to gain backward propulsion. Thus, the point force $\mathbf{f}$ is applied in the forward–downward direction (Figures 2g and 2h).

The $x$-direction and $z$-direction components of point force $\mathbf{f}$ can be determined from the force–balance equation (22) in the vertical ($z$-) and horizontal ($x$-) direction separately. The results are

$$f_x = \frac{6\pi\mu a V_{swimming}}{1 - \frac{1}{2}\left(\frac{3}{\beta} - \frac{1}{\beta^3}\right)} \quad (29)$$

for the $x$-direction component, and

$$f_z = \frac{-W_{excess}}{1 - \frac{1}{4}\left(\frac{3}{\beta} + \frac{1}{\beta^3}\right)} \quad (30)$$

for the $z$-direction component, where $\beta = (a + a/2)/a = 1.5$.

For the excess weight $\mathbf{W}_{excess} = -5.77 \times 10^{-8}\,\mathbf{k}$ N, if $\mathbf{V}_{swimming} = -1.1\mathbf{i}$ mm s$^{-1}$ (one-quarter of the terminal velocity), $f_x = 9.727 \times 10^{-8}$ N and $f_z = -1.355 \times 10^{-7}$ N, and if $\mathbf{V}_{swimming} = -4.4\mathbf{i}$ mm s$^{-1}$ (the terminal velocity), $f_x = 3.891 \times 10^{-7}$ N and $f_z = -1.355 \times 10^{-7}$ N.

*Forward swimming model*

When the model copepod swims horizontally forward (positive $x$-direction) with velocity $V_{swimming}\mathbf{i}$, the point force $\mathbf{f}$ has to be applied in the backward-downward direction (Figures 2i and 2j). The reason is that while the copepod pushes water downward to overcome the excess weight, it has to simultaneously push water backward in order to

**Fig. 2.** The free body diagram for a spherical copepod (**a**) hovering (like a helicopter) in the water, (**c**) sinking freely through the water, (**e**) swimming upward in the water, (**g**) swimming backward in the water, and (**i**) swimming forward in the water. In order to understand the way that the spherical copepod applies unbalanced forces to its surrounding water and generate a flow field around its body, the free body diagram for the water surrounding the spherical copepod (**b**) hovering in the water, (**d**) sinking freely through the water, (**f**) swimming upward in the water, (**h**) swimming backward in the water, and (**j**) swimming forward in the water is also drawn. **W** stands for the copepod's weight acting at the centre of mass; **B** stands for the buoyancy acting at the centre of volume; $\mathbf{f}'$ is the reaction force by the water acting on the appendages; **F** stands for the drag force by the surrounding water flow over the surface of the body; **f** is the point force exerted on the water by the copepod, representing the effect of the beating movement of cephalic appendages; $\mathbf{F}'$ stands for the force by the copepod on the surrounding water over the body-fluid interface. Note that (due to Newton's third law) $\mathbf{f}' = -\mathbf{f}$, and $\mathbf{F}' = -\mathbf{F}$.

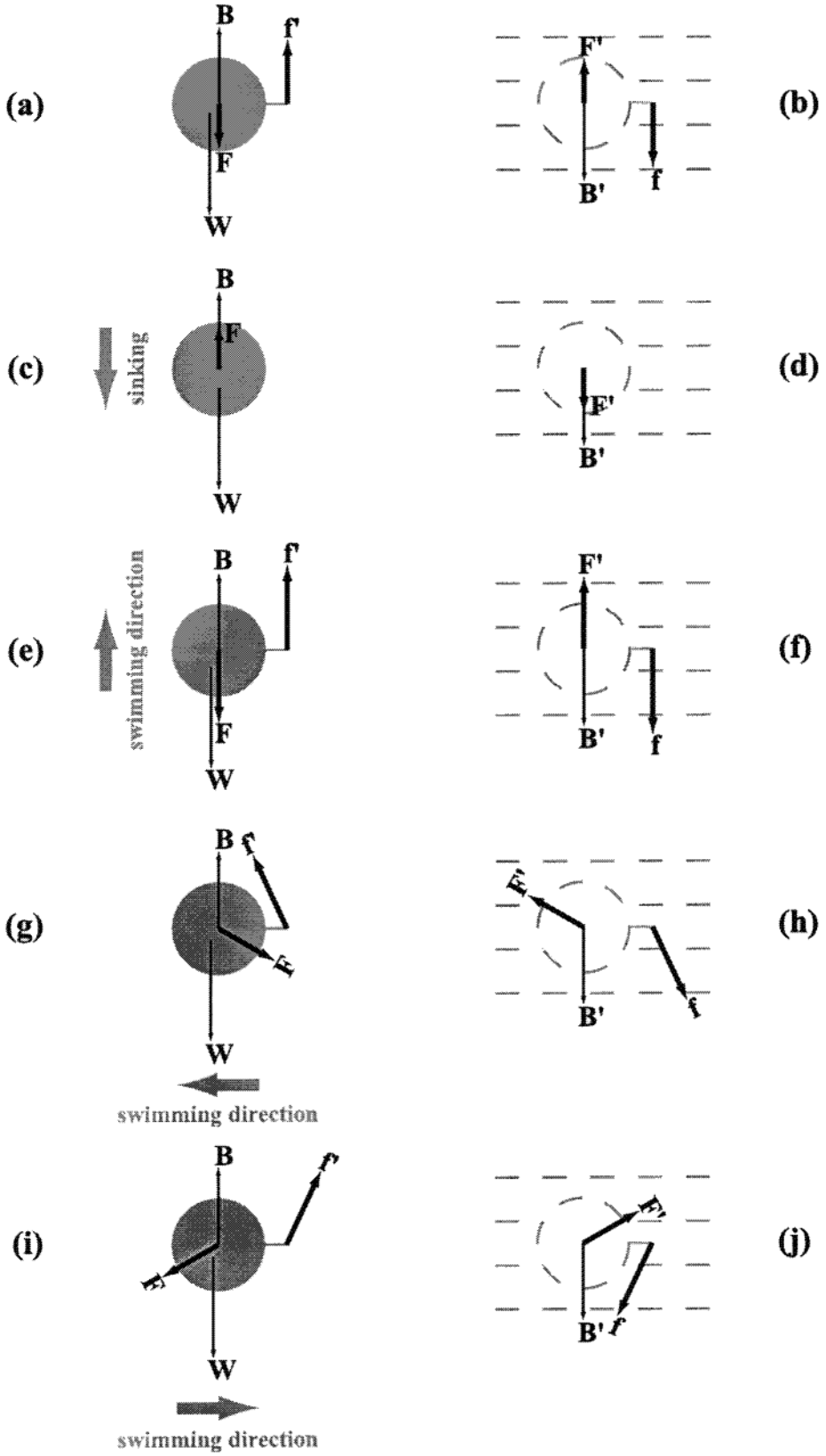
(a)
B
f'
F
W
(b)
F'
B'
f
(c)
sinking
B
F
W
(d)
F'
B'
(e)
swimming direction
B
f'
F
W
(f)
F'
B'
f
(g)
B
f'
F'
W
swimming direction
(h)
F'
B'
f
(i)
B
f'
F'
W
swimming direction
(j)
F'
B'
f

gain forward propulsion.

The $x$-direction and $z$-direction components of the point force $\mathbf{f}$ can be determined from equations (29) and (30), respectively. For the excess weight $\mathbf{W}_{excess} = -5.77 \times 10^{-8}\mathbf{k}$ N, if $\mathbf{V}_{swimming} = 1.1\mathbf{i}$ mm s$^{-1}$ (one-quarter of the terminal velocity), $f_x = -9.727 \times 10^{-8}$ N and $f_z = -1.355 \times 10^{-7}$ N, and if $\mathbf{V}_{swimming} = 4.4\mathbf{i}$ mm s$^{-1}$ (the terminal velocity), $f_x = -3.891 \times 10^{-7}$ N and $f_z = -1.355 \times 10^{-7}$ N.

Here, we provide some comments about the swimming velocity. When the model copepod swims at a low velocity (at least several times lower than the terminal velocity of the copepod), it turns out that the point force $\mathbf{f}$ representing the effect of the beating movement of the cephalic appendages does not deviate too much from that of the hovering model. For example, if the model copepod swims at a speed of 1.1 mm s$^{-1}$ (one-quarter of the terminal velocity), the magnitude of the point force calculated for the upward swimming model is $1.693 \times 10^{-7}$ N, which is not far from the value for the hovering model. On the other hand, when the model copepod swims at a velocity equal to or greater than the terminal velocity, it turns out that the point force $\mathbf{f}$ deviates significantly from that of the hovering model. As will be seen in the following section, this distinction has profound effects on the geometry of the flow field around a copepod.

## MODEL RESULTS

In the previous section, five Stokes flow models have been proposed to model the flow around a spherical copepod with various swimming behaviours. Given the excess weight and the swimming behaviour as well as the swimming velocity, the flow field around the copepod in steady motion can be analytically determined through the equation (21). In this section, we describe the model results for eight cases: a case for the hovering model, a case for the freely sinking model, two cases for the upward swimming model, two cases for the backward swimming model, and two cases for the forward swimming model. For the latter three swimming models, the two cases considered are slow-swimming at a velocity of 1.1 mm s$^{-1}$ (one-quarter of the terminal velocity) and fast-swimming at a velocity of 4.4 mm s$^{-1}$ (equal to the terminal velocity).

### Flow geometry

The geometry of the flow field around a copepod can be visualized by constructing the streamtube through the capture area of the copepod (Jiang *et al.*, 1999). [The capture area of a copepod was defined in (Strickler, 1985).] In the present work, the capture area is defined for the spherical model copepod as the area enclosed by a small horizontal circle of radius 0.25 mm centred at the point (0.85 mm, 0.0, 0.2 mm). The circle is in a $xy$-plane. The frame of reference is fixed on the copepod, so that the velocity field $\mathbf{u}$ calculated from equation (21) is steady and the fluid particle trajectory coincides with the streamline passing through a same position in the flow field. Based on the calculated velocity field $\mathbf{u}$, fluid particle locations $\mathbf{x}^p(t)$ are determined by integrating numerically

$$\frac{d\mathbf{x}^p}{dt} = \mathbf{u}\left(\mathbf{x}^p\right) \tag{31}$$

The time integration scheme for equation (31) is a fourth-order Runge–Kutta method. Specifically, 40 points located on the circle enclosing the capture area are chosen as the initial conditions for the numerical integration. Then, backward integration of equation (31) in time determines the particle trajectories leading to the capture area, i.e. we determine from where the fluid particles that end up in the capture area have come. For the present work, the time integration is from 0 s to –2.5 s. The union of such trajectories forms the streamtube.

The streamtubes are calculated as a three-dimensional structure, however a two-dimensional lateral view is enough to show the difference among the eight cases (Figures 3–7). For the hovering case, the streamtube is cone-shaped and wide; in 2.5 s it transports water from 4 mm above and 2 mm in front of the copepod to the capture area (Figure 3). For the free-sinking case, since the water passes through the capture area from below, the streamtube is observed coming from below. At the beginning, the streamtube goes almost straight upward towards the copepod; when approaching the copepod, it travels along the copepod's ventral curvature. Compared to the hovering case, the streamtube is narrower and much longer (8 mm as shown in Figure 4). For the slow-upward swimming case (i.e. swimming at a velocity of 1.1 mm s$^{-1}$), the streamtube is cone-shaped and wide, entraining water from above as well as in front to the capture area (Figure 5a). Compared to the hovering case, the streamtube is just a little longer and narrower for a same period of time, because of the slow-upward translating motion. For the fast-upward swimming case (i.e. swimming at a velocity of 4.4 mm s$^{-1}$), the streamtube is quite narrow in comparison with the slow-upward swimming case and the hovering case. Generally, the streamtube is not cone-shaped; instead it is cylindrical and long (14 mm as shown in Figure 5b), due to the fast translating motion of the copepod. Figures 6a and 6b show, respectively, the streamtubes for the two cases of the backward swimming copepod, i.e. the slow-swimming case of velocity 1.1 mm s$^{-1}$ and the fast-swimming case of velocity 4.4 mm s$^{-1}$. The streamtube of the slow-swimming copepod is cone-shaped and wide, transporting water from behind and above the copepod (Figure 6a). On the other hand, for the fast-swimming case, the streamtube is narrow and not

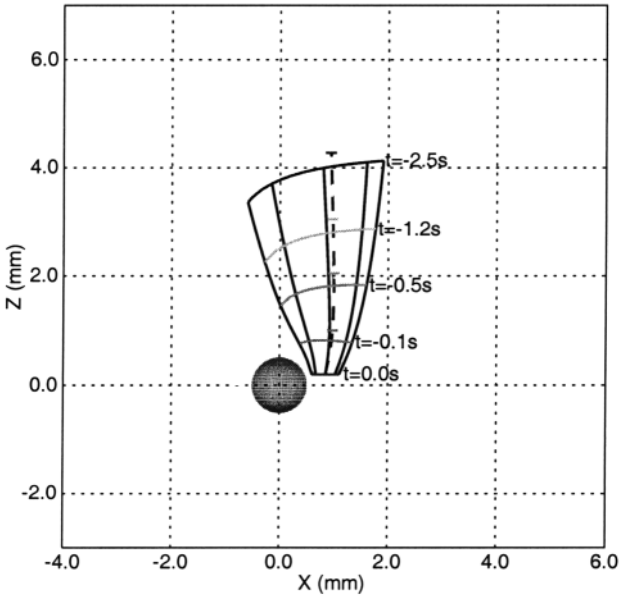


**Fig. 3.** Lateral view of the streamtube through the capture area of a spherical copepod hovering (like a helicopter) in the water. The dashed line is the streamline passing through the centre of the capture area.

cone-shaped, though it directs water from an even further distance behind and above the copepod (11 mm as shown in Figure 6b). Similar observations are obtained for the two cases of the forward swimming copepod: The streamtube of the slow-forward swimming copepod (with a swimming velocity of 1.1 mm $s^{-1}$) is cone-shaped and wide, entraining water from in front of and above the copepod (Figure 7a). While the streamtube of the fast-forward swimming copepod (with a swimming velocity of 4.4 mm $s^{-1}$) is not cone-shaped but narrow and long (13 mm as shown in Figure 7b).

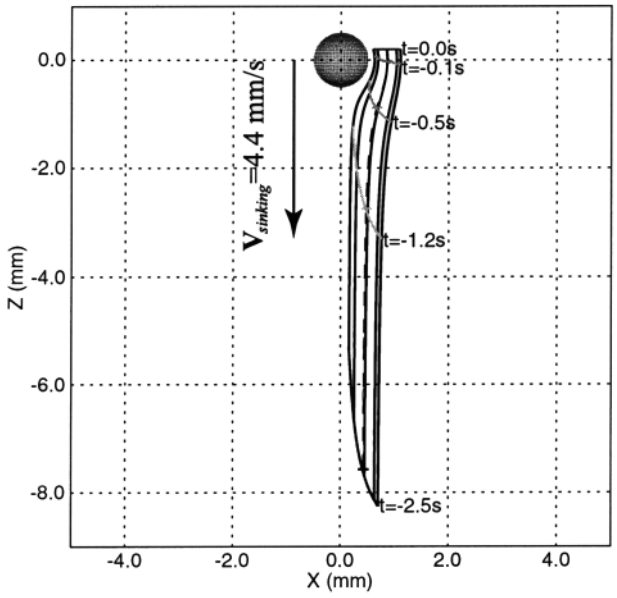


**Fig. 4.** Lateral view of the streamtube through the capture area of a spherical copepod sinking freely (i.e. in negative $z$-direction) at its terminal velocity (4.4 mm $s^{-1}$ for the present study). Note that the frame of reference is fixed on the copepod. The dashed line is the streamline passing through the centre of the capture area.

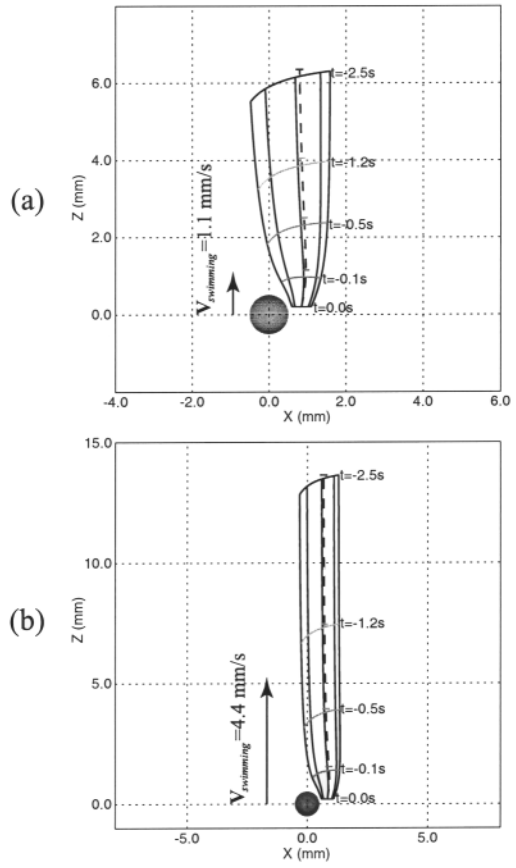


**Fig. 5.** Lateral view of the streamtube through the capture area of a spherical copepod swimming upward (i.e. in positive $z$-direction) (**a**) at a speed of 1.1 mm·$s^{-1}$, (**b**) at a speed of 4.4 mm $s^{-1}$. Note that the frame of reference is fixed on the copepod. The dashed line is the streamline passing through the centre of the capture area.

## Contour plots of velocity magnitudes

Using the fluid velocity components calculated from equation (21) in a Cartesian coordinate system, one can calculate the velocity magnitudes according to $|\mathbf{u}| = \sqrt{u_1^2 + u_2^2 + u_3^2}$. The contour plots of the velocity magnitudes along the horizontal plane $z = 0$ and along the vertical plane $y = 0$ are drawn for three cases, i.e. hovering (in Figure 8), slow-backward swimming at a velocity of 1.1 mm $s^{-1}$ (in Figure 9), and fast-backward swimming at a velocity of 4.4 mm $s^{-1}$ (in Figure 10). The contour plots show how the spatial configurations of the flow field

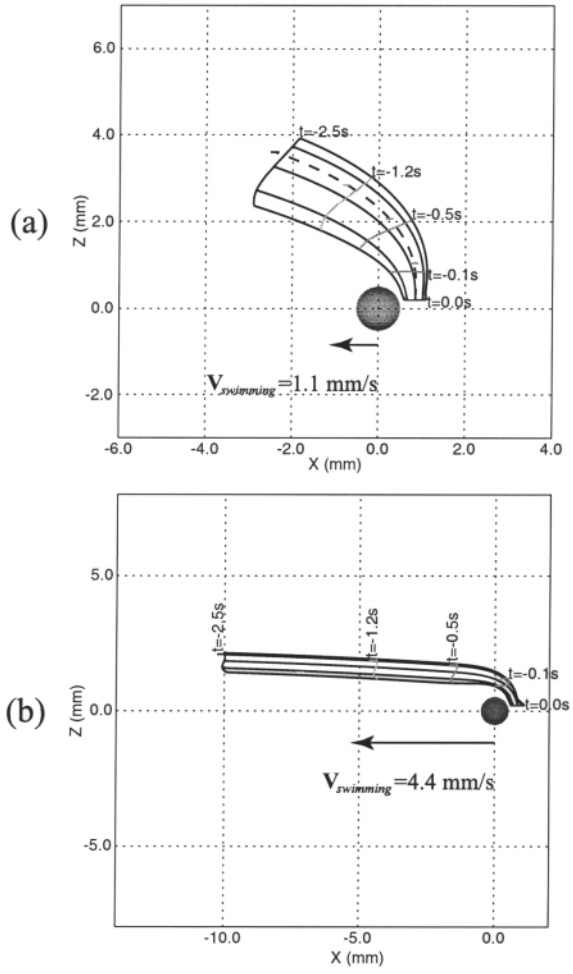


**Fig. 6.** Lateral view of the streamtube through the capture area of a spherical copepod swimming backward (i.e. in negative *x*-direction) (**a**) at a speed of 1.1 mm $s^{-1}$, (**b**) at a speed of 4.4 mm $s^{-1}$. Note that the frame of reference is fixed on the copepod. The dashed line is the streamline passing through the centre of the capture area.

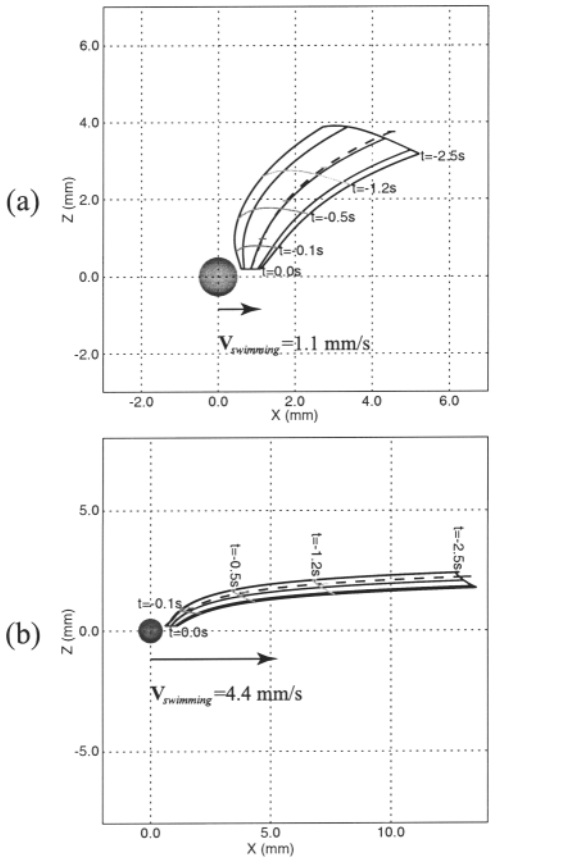


**Fig. 7.** Lateral view of the streamtube through the capture area of a spherical copepod swimming forward (i.e. in positive *x*-direction) (**a**) at a speed of 1.1 mm $s^{-1}$, (**b**) at a speed of 4.4 mm $s^{-1}$. Note that the frame of reference is fixed on the copepod. The dashed line is the streamline passing through the centre of the capture area.

change with different swimming behaviours.

## DISCUSSION

### Swimming behaviour and flow geometry

One of the purposes of the present work is to find out how the swimming behaviour controls the geometry of the flow field generated by a freely swimming copepod. Generally speaking, the streamtube associated with a copepod swimming slowly (i.e. swimming at a speed at least several times smaller than the terminal velocity of the copepod, termed the slow-swimming behaviour) resembles the streamtube of a copepod hovering in the water. In both situations of hovering and swimming slowly, the streamtube is cone-shaped and wide (Figures 3, 5a, 6a and 7a), transporting water to the capture area, and the flow field generated by the copepod is usually termed 'the feeding current'. This conclusion is consistent with the laboratory-observed swimming behaviour of calanoid copepods listed in Table I, in which many species that display hovering or slow-swimming or drifting behaviour generate a feeding current. The wide and cone-shaped streamtube may correspond to the viscous core hypothesis by Strickler (Strickler, 1985). In contrast, when a copepod swims at a speed equal to or greater than the terminal velocity (termed the fast-swimming behaviour), the streamtube through the capture area is narrow, long and not cone-shaped (Figures 5b, 6b and 7b). Thus, the flow field around a fast-swimming copepod is not like a feeding current, though it still transports water to the capture area. This conclusion is also consistent with the laboratory-

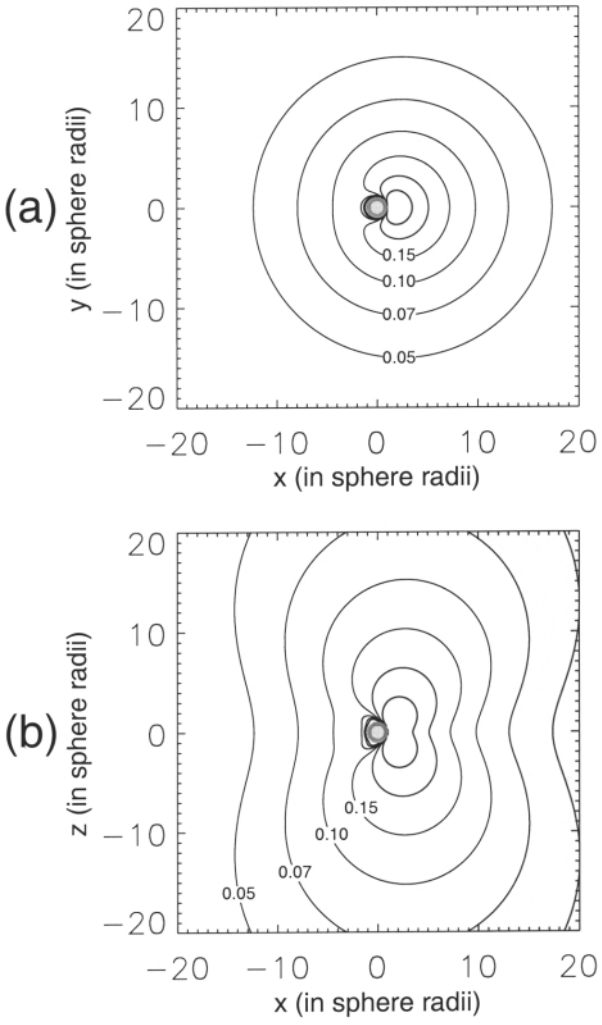


**Fig. 8.** Contour plots of velocity magnitudes of the flow field around a hovering copepod. The velocity magnitudes have been normalized by the terminal velocity of the copepod (4.4 mm $s^{-1}$ for the present study). (**a**) along the plane $z = 0$; (**b**) along the plane $y = 0$.

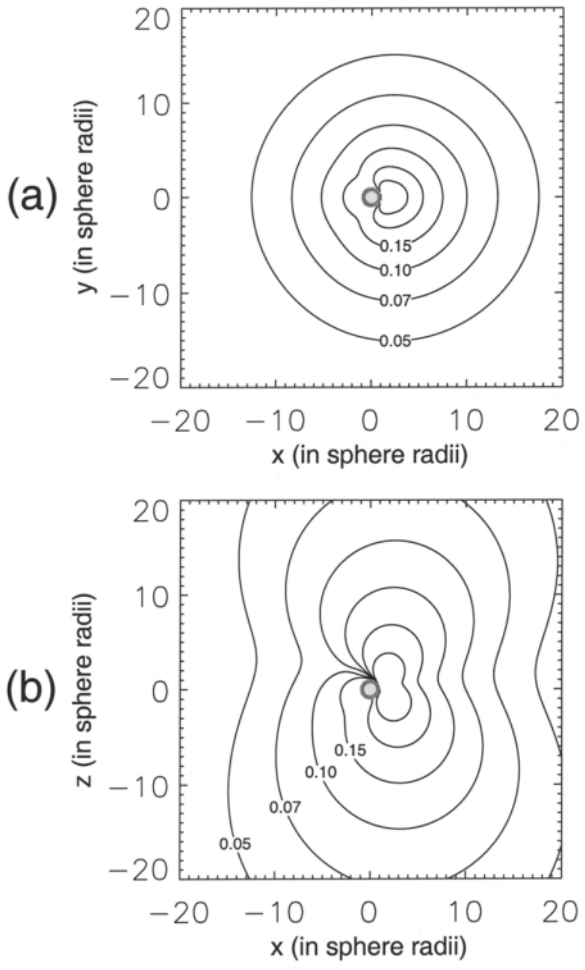


**Fig. 9.** Contour plots of velocity magnitudes of the flow field around a backward swimming copepod in a stationary frame of reference. The copepod swims in the negative $x$-direction at a speed of 1.1 mm $s^{-1}$. The velocity magnitudes have been normalized by the terminal velocity of the copepod (4.4 mm $s^{-1}$ for the present study). (**a**) along the plane $z = 0$; (**b**) along the plane $y = 0$.

observed swimming behaviour of calanoid copepods listed in Table I, in which many species that swim in a fast fashion, eliciting raptorial behaviour, do not generate a feeding current. The narrow, long and non-cone-shaped streamtube may correspond to the motion core hypothesis by Strickler (Strickler, 1985). In addition, when a copepod sinks freely (Figure 4), the flow comes from below relative to the copepod and the streamtube through the capture area is narrower and longer than hovering or swimming slowly, but shorter than swimming fast. Again, the flow field around a freely sinking copepod is not like a feeding current. Correspondingly, the contour plots of velocity magnitudes show that the hovering case and the slow-swimming cases have a quite similar spatial configuration in the flow field (Figures 8 and 9). However, the flow field of the fast-swimming cases deviates substantially from the hovering case, as can be seen by comparing Figure 10 with Figure 8.

These results may shed light on why calanoid copepods exhibit a wide range of variable swimming behaviours. Since the swimming behaviour controls the flow geometry, through adopting certain swimming behaviour a calanoid copepod may be able to control the geometry of the flow field around its body and such flow geometry may enable the copepod to realize certain ecological functions. These ecological functions may include chemoreception, mechanoreception, feeding, and predator avoidance etc. Apparently, 'the feeding current' benefits a copepod's suspension feeding. On the other hand, when a copepod swims fast, there exists a strong shear layer (flow distortion)

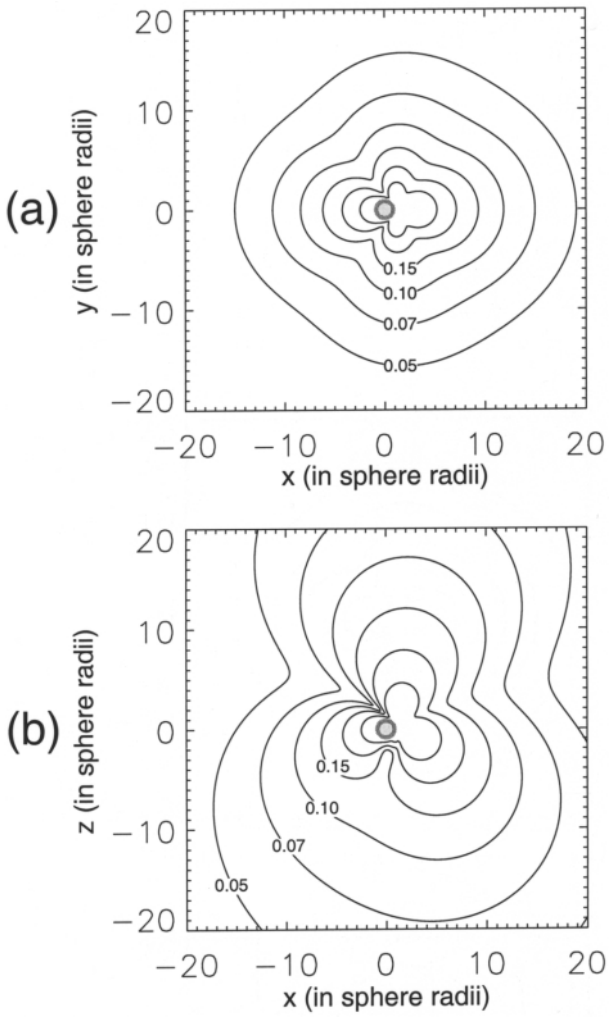


**Fig. 10.** Contour plots of velocity magnitudes of the flow field around a backward swimming copepod in a stationary frame of reference. The copepod swims in the negative $x$-direction at a speed of 4.4 mm $s^{-1}$. The velocity magnitudes have been normalized by the terminal velocity of the copepod (4.4 mm $s^{-1}$ for the present study). (**a**) along the plane $z = 0$; (**b**) along the plane $y = 0$.

at the side of the swimming direction and above the copepod (see Figure 10b; i.e. at the place where the antennules locate). Such flow configuration benefits the mechanoreception of the copepod. By swimming fast, *Centropages* intentionally creates a narrow feeding current that works in this way (Bundy and Paffenhöfer, 1996).

## Terminal velocity as a natural velocity scale

Calanoid copepods come in a wide range of sizes, shapes and swimming velocities, and are usually slightly heavier than sea water (so that they will sink when they stop beating their cephalic appendages). How can we distinguish between slow-swimming and fast-swimming among species? In this section, we discuss how to scale the swimming velocity of different copepod species. We argue that the terminal velocity of copepods is the most natural scaling. The flow field around a freely swimming copepod can be divided into two parts: the part due to the requirement to counterbalance the excess weight and the part due to the self-propelled swimming (i.e. due to the requirement to counterbalance the drag force resulting from swimming). For the present work, which uses Stokes flow models to describe the flow field around a freely swimming spherical copepod, the part of the flow field due to the requirement to counterbalance the excess weight is the flow field around a spherical copepod hovering in the water (as shown in Figure 8). This part looks like the flow generated by a force monopole. The rest of the flow is the part due to the self-propelled swimming with various behaviours (examples are shown in Figure 11; i.e. for the situations of neutral buoyancy). Generally, this part looks like the flow field generated by a force dipole [see (Childress, 1981)], because the copepod applies both drag force and propulsion on the water. When a copepod swims

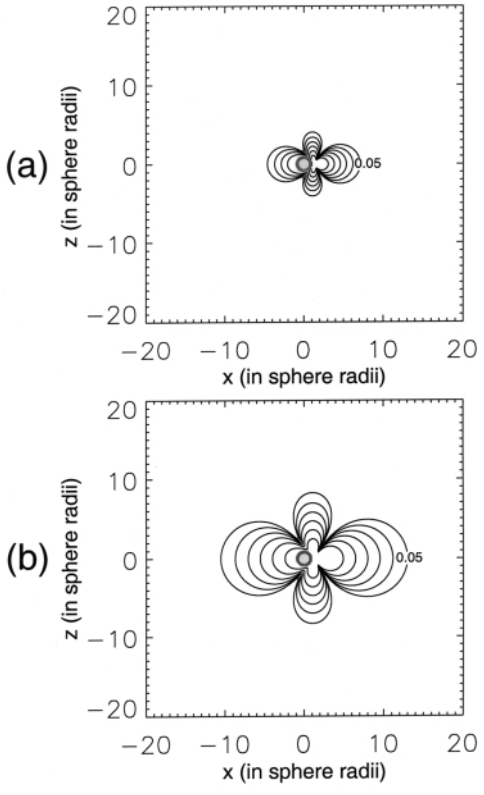


**Fig. 11.** Contour plots of velocity magnitudes of the part, due to the self-propelled swimming, of the flow field around a backward swimming copepod in a stationary frame of reference. The plots are drawn along the plane $y = 0$, and the velocity magnitudes have been normalized by the terminal velocity of the copepod (4.4 mm $s^{-1}$ for the present study). The copepod swims in the negative $x$-direction at a speed of (**a**) 1.1 mm $s^{-1}$, and (**b**) 4.4 mm $s^{-1}$.

slowly (i.e. to swim at a speed at least several times lower than the free-sinking terminal velocity of the copepod, termed the slow-swimming behaviour), the part of the flow due to the self-propelled swimming is much weaker than that due to the requirement to counterbalance the excess weight (see Figure 12). In this situation, the requirement to counterbalance the excess weight is the dominant factor in generating the flow field around the copepod, and the geometry of the flow field is cone-shaped and wide, resembling the geometry of the flow field around a copepod hovering in the water. In contrast, when a copepod swims fast (i.e. to swim at a speed comparable to or greater than its terminal velocity, termed the fast-swimming behaviour), in the near field, the part of the flow due to the self-propelled swimming is comparable to or stronger than that due to the requirement to counterbalance the excess weight (see Figure 12), and the copepod puts its energy far more into propulsion than into drawing water towards it. As a result, swimming of the copepod is the dominant factor in generating the flow field, and the flow field deviates very much from the flow field around a hovering copepod and is not like a feeding current.

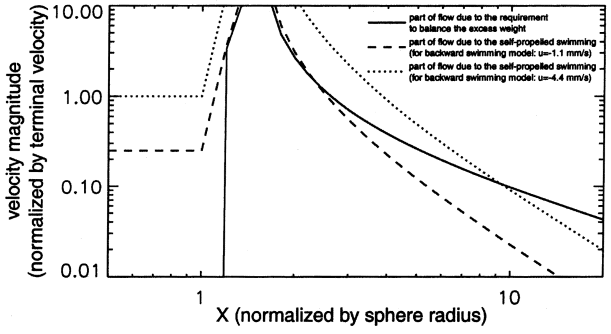


**Fig. 12.** The velocity decay along the line $y = 0$, $z = 0$ for the parts of the flow field around a copepod swimming backward: at a velocity of 1.1 mm $s^{-1}$ and of 4.4 mm $s^{-1}$. The velocity magnitudes have been normalized by the terminal velocity of the copepod (4.4 mm $s^{-1}$ for the present study).

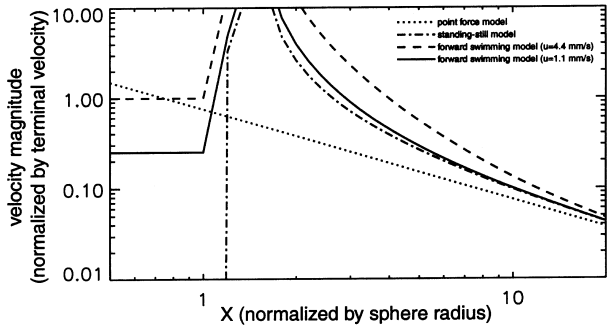


**Fig. 13.** The velocity decay along the line $y = 0$, $z = 0$ for different models. (Here, the standing-still model refers to the hovering model). The velocity magnitudes have been normalized by the terminal velocity of the copepod (4.4 mm $s^{-1}$ for the present study).

Our argument is supported by some observations shown in Table I. A *Clausocalanus furcatus* female swam fast, at a mean speed of about 10 mm $s^{-1}$, which is five times greater than its free-sinking terminal velocity of 2 mm $s^{-1}$; this species does not generate a feeding current (Mazzocchi and Paffenhöfer, 1999). By contrast, a *Pseudocalanus elongatus* female swam slowly at a velocity 0.5 mm $s^{-1}$, which is half its terminal velocity of 1.1 mm $s^{-1}$; this species generates a feeding current (Tiselius and Jonsson, 1990).

## Velocity decay

The velocity of the flow field around a freely swimming copepod decays with increasing distance away from the copepod. Since the flow field due to a force monopole decays in the order of $1/r$ while the flow field due to a force dipole decays in the order of $1/r^2$ (where $r$ is the distance measured from the pole), only the effect of the excess weight (force monopole) will be seen in the far field. Hence, the velocity field decays in the far field to the velocity field generated by a point force of magnitude of the excess weight in an infinite domain. Figure 13 clearly shows that the velocity magnitudes of various models (e.g. the hovering model and the forward swimming model with swimming velocity 4.4 mm $s^{-1}$ or 1.1 mm $s^{-1}$) decay to the velocity field generated by a point force. Here, the velocity field generated by the point force is calculated according to equations (12) and (13) by simply replacing $\mathbf{f}$ with the excess weight $\mathbf{W}_{excess}$ of the copepod. For the purpose of comparison, we also show the contour plots of the velocity field of this point force model in Figure 14, which has a spatial configuration almost exactly identical to the freely sinking model, and deviates little from the hovering model.

## A freely swimming copepod is a self-propelled body

In order to show the significance of the fact that a freely swimming copepod is a self-propelled body, we also compare the decays of our models to the so-called towed body model. The towed body model is the Stokes flow field due to the translating motion of a solid sphere. It is clearly shown in Figure 15 that the decay of the velocity field of the towed body model depends on the translating velocity of the sphere, unlike our self-propelled body models that decay in the far field to the point force model regardless of the swimming velocity of the body. We also compare the velocity fields calculated from the towed body model to those calculated from the self-propelled body models in Figure 16 to see further the difference between the towed body model and our self-propelled body models. For the towed body model, the velocity maximum (equal to the swimming velocity) is reached at

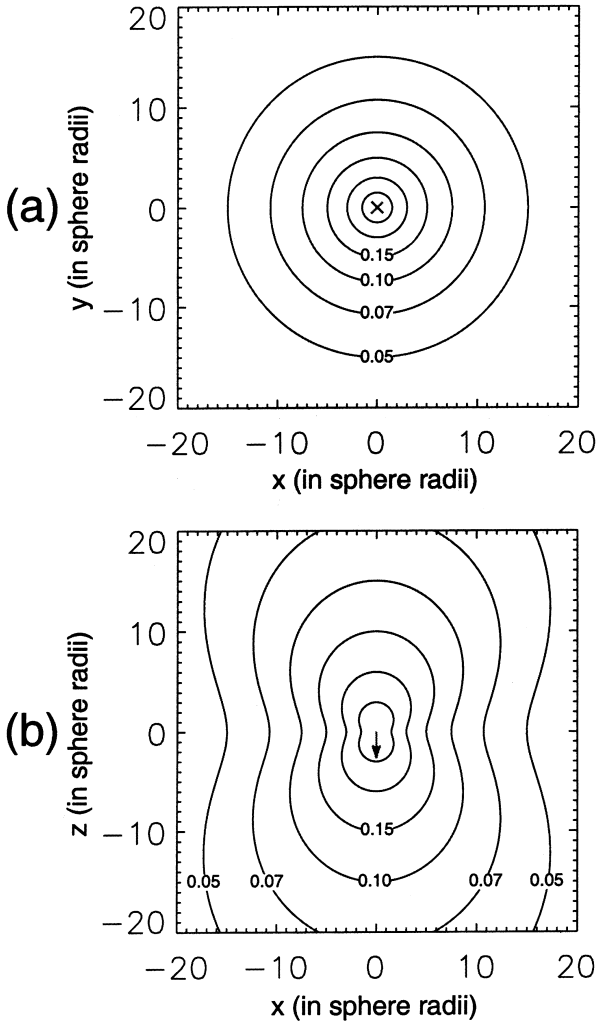


**Fig. 14.** Contour plots of velocity magnitudes of the point force model. The point force is located at the origin and in negative $z$-direction with a magnitude of the excess weight of the spherical copepod ($5.77 \times 10^{-8}$ N for the present study). The velocity magnitudes have been normalized by the terminal velocity of the copepod (4.4 mm $s^{-1}$ for the present study). (**a**) along the plane $z = 0$; (**b**) along the plane $y = 0$.

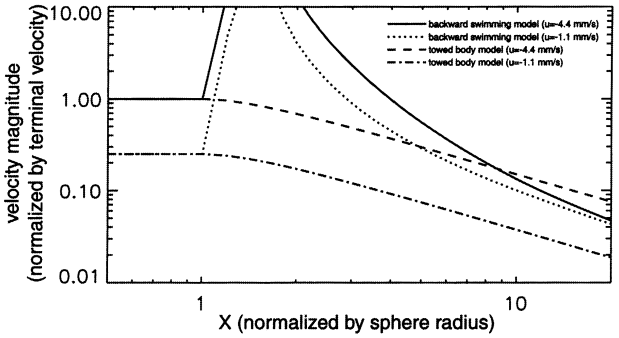


**Fig. 15.** The velocity decay along the line $y = 0$, $z = 0$ for the towed body model and the backward swimming (self-propelled body) model. For the towed body model, the translating velocity of the sphere is in negative $x$-direction, as for the backward swimming model. The velocity magnitudes have been normalized by the terminal velocity of the copepod (4.4 mm $s^{-1}$ for the present study).

the body surface when using a stationary frame of reference (Figures 16a and 16c). While, a freely swimming copepod was observed to generate a flow field with areas of high velocity (larger than the swimming velocity) located in a short distance away from the body surface, and in most situations ventrally or anterior–ventrally to the body surface (Bundy and Paffenhöfer, 1996). Apparently, our self-propelled body models have the ability to reproduce this important characteristic of the flow field generated by a freely swimming copepod (Figures 16b and 16d, see also Figures 8–10). Owing to its inability to reproduce the self-propelled characteristic of a freely swimming copepod, the towed body model should not be used to describe the flow field around a freely swimming copepod.

## Conclusions

The geometry of the flow field around a freely swimming copepod varies significantly for different swimming behaviours. The streamtube through the capture area of a copepod swimming slowly (i.e. swimming at a speed at least several times lower than the free-sinking terminal velocity of the copepod) resembles the streamtube of a copepod hovering in the water. For the swimming behaviour of hovering or swimming slowly, the streamtube is cone-shaped and wide, transporting water to the capture area, and the copepod generates a feeding current. In contrast, when a copepod swims fast (i.e. at a speed equal to or greater than the terminal velocity), the streamtube through the copepod's capture area is cylindrical, narrow, long and not cone-shaped. In addition, when a copepod sinks freely, the flow comes from below relative to the copepod and the streamtube through the capture area is narrower and longer than hovering and swimming slowly but shorter than swimming fast. The flow field around a fast-swimming or free-sinking copepod is not like a feeding current. The differences in the flow geometry with the different swimming behaviours are due to the relative importance between the two factors in generating the flow field: the copepod's swimming motion and the requirement to counterbalance the copepod's excess weight.

The terminal velocity of a copepod provides a natural velocity scale for describing the swimming and associated flow field around the copepod. When a copepod swims at a speed at least several times smaller than the terminal velocity of the copepod, the behaviour is termed the slow-

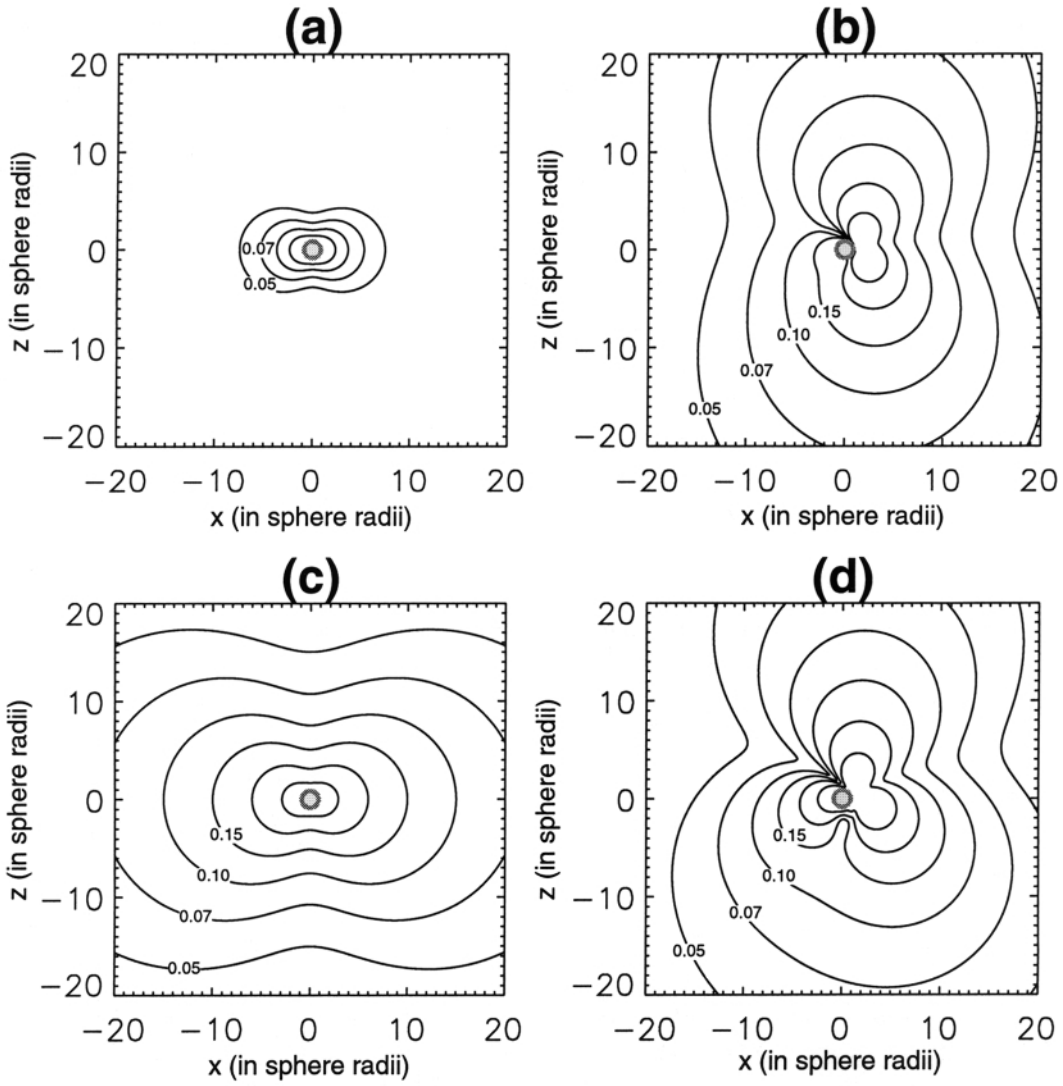


**Fig. 16.** Contour plots of velocity magnitudes of the flow field calculated from (**a**) and (**c**) the towed body model and (**b**) and (**d**) the self-propelled body model. The plots are drawn along the plane $y = 0$ and the velocities have been calculated using a stationary frame of reference and the velocity magnitudes normalized by 4.4 mm $s^{-1}$ (the terminal velocity of the spherical copepod). In (**a**), the sphere (a towed body) translates in the negative $x$-direction at a speed of 1.1 mm $s^{-1}$. In (**b**), the spherical copepod (a self-propelled body) swims backward in the negative $x$-direction at a speed of 1.1 mm $s^{-1}$. In (**c**), the sphere (a towed body) translates in the negative $x$-direction at a speed of 4.4 mm $s^{-1}$. In (**d**), the spherical copepod (a self-propelled body) swims backward in the negative $x$-direction at a speed of 4.4 mm $s^{-1}$.

swimming behaviour. By contrast, when a copepod swims at a speed equal to or greater than the terminal velocity, the behaviour is termed the fast-swimming behaviour.

That a freely swimming copepod is a self-propelled body is a fundamental factor for simulating the flow field around the copepod. 'Self-propelled' means a freely swimming copepod must gain thrust from the surrounding water in order to counterbalance the drag force by water and its excess weight. Regardless of swimming behaviours and velocities, the far-field velocity field decays to that of the velocity field generated by a point force of magnitude equal to the copepod's excess weight, in an infinite domain. On the other hand, the towed body model to describe the flow field around a copepod yields much different far- and near-field flow characteristics. Hence, the towed body model is inherently unable to reproduce fundamental characteristics of the flow field around a freely swimming copepod.

Finally, we point out that in the far field the actual flow at finite Reynolds number is expected to deviate from the present Stokes flow results since even at very low *Re*, there exists a distance from the body at which inertia-forces

become larger than viscous ones (Panton, 1996). The present work using Stokes flow models can only provide some general insights of how the swimming behaviour of a copepod controls the flow field around it. In order to consider further the effects of morphology, body orientation, energetics and feeding efficiency, numerical simulations to solve the full steady Navier–Stokes equations with a realistic body shape are needed. The required numerical simulations and results are described in a companion paper (Jiang *et al.*, 2002).

## ACKNOWLEDGMENTS

The authors would like to thank Professor C. Pozrikidis for providing the subroutine for calculating the Green's function for an infinite flow bounded internally by a solid sphere. Thanks are due to Professor A. Prosperetti for offering useful references on Stokes flow. We are grateful to Professor J. R. Strickler and an anonymous reviewer for very helpful comments on the manuscript. The financial support of the Office of Naval Research (contract number N000149710429) is gratefully acknowledged.

## REFERENCES

Alcaraz, M., Paffenhöfer, G.-A. and Strickler, J. R. (1980) Catching the algae: A first account of visual observations on filter-feeding calanoids. In Kerfoot, W. C. (ed.), *Evolution and Ecology of Zooplankton Communities, American Society of Limnology and Oceanography Special Symposium*. University Press of New England, Hanover, NH and London, UK, Vol. 3, pp. 241–248.

Bundy, M. H. and Paffenhöfer, G.-A. (1996) Analysis of flow fields associated with freely swimming calanoid copepods. *Mar. Ecol. Prog. Ser.*, **133**, 99–113.

Bundy, M. H., Gross, T. F., Coughlin, D. J. and Strickler, J. R. (1993) Quantifying copepod searching efficiency using swimming pattern and perceptive ability. *Bull. Mar. Sci.*, **53**, 15–28.

Cannon, H. G. (1928) On the feeding mechanism of the copepods, *Calanus finmarchicus* and *Diaptomus gracilis*. *Br. J. Exp. Biol.*, **6**, 131–144.

Childress, S. (1981) *Mechanics of Swimming and Flying*. Cambridge University Press, Cambridge. 155 pp.

Conover, R. J. (1968) Zooplankton—Life in a nutritionally dilute environment. *Am. Zool.*, **8**, 107–118.

Cowles, T. J. and Strickler, J. R. (1983) Characterization of feeding activity patterns in the planktonic copepod *Centropages typicus* Kroyer under various food conditions. *Limnol. Oceanogr.*, **28**, 105–115.

Esterly, C. O. (1916) The feeding habits and food of pelagic copepods, and the question of nutrition by organic substances in solution in the water. *Univ. Calif. Publ. Zool.*, **16**, 171–184.

Fields, D. M. and Yen, J. (1993) Outer limits and inner structure: The 3-dimensional flow fields of *Pleuromamma xiphias*. *Bull. Mar. Res.*, **53**, 84–95.

Fields, D. M. and Yen, J. (1997) Implications of the feeding current structure of *Euchaeta rimana*, a carnivorous pelagic copepod, on the spatial orientation of their prey. *J. Plankton Res.*, **19**, 79–95.

Gauld, D. T. (1966) The swimming and feeding of planktonic copepods. In Barnes, H. (ed.) *Some Contemporary Studies in Marine Science*. George Allen and Unwin Ltd., London, pp. 313–334.

Gill, C. W. (1987) Recording the beat patterns of the second antennae of calanoid copepods, with a micro-impedance technique. *Hydrobiologia*, **148**, 73–78.

Greene, C. H. (1988) Foraging tactics and prey-selection patterns of omnivorous and carnivorous calanoid copepods. *Hydrobiologia*, **167/168**, 295–302.

Greene, C. H. and Landry, M. R. (1985) Patterns of prey selection in the cruising calanoid predator *Euchaeta elongata*. *Ecology*, **66**, 1408–1416.

Greene, C. H. and Landry, M. R. (1988) Carnivorous suspension feeding by the subarctic calanoid copepod *Neocalanus cristatus*. *Can. J. Fish. Aquat. Sci.*, **45**, 1069–1074.

Higdon, J. J. L. (1979) A hydrodynamic analysis of flagellar propulsion. *J. Fluid Mech.*, **90**, 685–711.

Huys, R. and Boxshall, G. A. (1991) *Copepod Evolution*. The Ray Society, London. 468 pp.

Hwang, J.-S. and Turner, J. T. (1995) Behaviour of cyclopoid, harpacticoid, and calanoid copepods from coastal waters of Taiwan. *P.S.Z.N. I: Marine Ecology*, **16**, 207–216.

Jiang, H., Meneveau, C. and Osborn, T. R. (1999) Numerical study of the feeding current around a copepod. *J. Plankton Res.*, **21**, 1391–1421.

Jiang, H., Meneveau, C. and Osborn, T. R. (2002) The flow field around a freely swimming copepod in steady motion: Part II Numerical simulation. *J. Plankton Res.*, **24**, 191–213.

Jonsson, P. R. and Tiselius, P. (1990) Feeding behaviour, prey detection and capture efficiency of the copepod *Acartia tonsa* feeding on planktonic ciliates. *Mar. Ecol. Prog. Ser.*, **60**, 35–44.

Jørgensen, C. B. (1966) *Biology of Suspension Feeding*. Pergamon Press, Oxford. 357 pp.

Koehl, M. A. R. and Strickler, J. R. (1981) Copepod feeding currents: Food capture at low Reynolds number. *Limnol. Oceanogr.*, **26**, 1062–1073.

Landau, L. D. and Lifshitz, E. M. (1959) *Fluid Mechanics*. Pergamon Press. 536 pp.

Lowndes, A. G. (1935) The swimming and feeding of certain calanoid copepods. *Proceedings of the Zoological Society of London*, 687–715.

Mauchline, J. (1998) The Biology of Calanoid Copepods. *Adv. Mar. Biol.*, **33**, 1–710.

Mazzocchi, M. G. and Paffenhöfer, G.-A. (1999) Swimming and feeding behaviour of the planktonic copepod *Clausocalanus furcatus*. *J. Plankton Res.*, **21**, 1501–1518.

Paffenhöfer, G.-A. and Lewis, K. D. (1990) Perceptive performance and feeding behavior of calanoid copepods. *J. Plankton Res.*, **12**, 933–946.

Paffenhöfer, G.-A., Strickler, J. R. and Alcaraz, M. (1982) Suspension-feeding by herbivorous calanoid copepods: A cinematographic study. *Mar. Biol.*, **67**, 193–199.

Panton, R. L. (1996) *Incompressible Flow*. John Wiley & Sons, Inc., New York. 837 pp.

Pozrikidis, C. (1992) *Boundary Integral and Singularity Methods for Linearized Viscous Flow*. Cambridge University Press, Cambridge. 259 pp.

Pozrikidis, C. (1997) *Introduction to Theoretical and Computational Fluid Dynamics*. Oxford University Press, New York. 675 pp.

Price, H. J. and Paffenhöfer, G.-A. (1986a) Capture of small cells by the copepod *Eucalanus elongatus*. *Limnol. Oceanogr.*, **31**, 189–194.

Price, H. J. and Paffenhöfer, G.-A. (1986b) Effects of concentration on

the feeding of a marine copepod in algal monocultures and mixtures. *J. Plankton Res.*, **8**, 119–128.

Price, H. J., Paffenhöfer, G.-A. and Strickler, J. R. (1983) Modes of cell capture in calanoid copepods. *Limnol. Oceanogr.*, **28**, 116–123.

Stamhuis, E. J. and Videler, J. J. (1995) Quantitative flow analysis around aquatic animals using laser sheet particle image velocimetry. *J. Exp. Biol.*, **198**, 283–294.

Storch, O. and Pfisterer, O. (1925) Der Fangapparat von Diaptomus. *Zeitschrift für vergleichende Physiologie*, **3**, 330–376.

Strickler, J. R. (1982) Calanoid copepods, feeding currents, and the role of gravity. *Science*, **218**, 158–160.

Strickler, J. R. (1984) Sticky water: A selective force in copepod evolution. In Meyers, D. G and Strickler, J. R. (eds), *Trophic Interactions within Aquatic Ecosystems*. American Association for the Advancement of Science, Washington, D.C., pp. 187–239.

Strickler, J. R. (1985) Feeding currents in calanoid copepods: Two new hypotheses. In Lavarack, M. S. (ed.), Physiological Adaptations of Marine Animals. *Symp. Soc. Exp. Biol.*, **23**, 459–485.

Tiselius, P. and Jonsson, P. R. (1990) Foraging behaviour of six calanoid copepods: Observations and hydrodynamic analysis. *Mar. Ecol. Progr. Ser.*, **66**, 23–33.

Vanderploeg, H. A. and Paffenhöfer, G.-A. (1985) Modes of algal capture by the freshwater copepod *Diaptomus sicilis* and their relation to food-size selection. *Limnol. Oceanogr.*, **30**, 871–885.

van Duren, L. A., Stamhuis, E. J. and Videler, J. J. (1998) Reading the copepod personal ads: Increasing encounter probability with hydromechanical signals. *Phil. Trans. R. Soc. Lond.*, **B353**, 691–700.

Wong, C. K. (1988a) Effects of competitors, predators, and prey on the grazing behavior of herbivorous calanoid copepods. *Bull. Mar. Sci.*, **43**, 573–582.

Wong, C. K. (1988b) The swimming behavior of the copepod *Metridia pacifica*. *J. Plankton Res.*, **10**, 1285–1290.

Wong, C. K. and Sprules, W. G. (1986) The swimming behavior of the freshwater calanoid copepods *Limnocalanus macrurus* Sars, *Senecella calanoides* Juday and *Epischura lacustris* Forbes. *J. Plankton Res.*, **8**, 79–90.

Wong, C. K., Ramcharan, C. W. and Sprules, W. G. (1986) Behavioral responses of a herbivorous calanoid copepod to the presence of other zooplankton. *Can. J. Zool.*, **64**, 1422–1425.

Yen, J. (1988) Directionality and swimming speeds in predator-prey and male-female interactions of *Euchaeta rimana*, a subtropical marine copepod. *Bull. Mar. Sci.*, **43**, 395–403.

Yen, J. and Fields, D. M. (1992) Escape responses of *Acartia hudsonica* nauplii from the flow field of *Temora longicornis*. *Arch. Hydro. Beih.*, **36**, 123–134.

Yen, J. and Strickler, J. R. (1996) Advertisement and concealment in the plankton: What makes a copepod hydrodynamically conspicuous? *Invert. Biol.*, **115**, 191–205.

Yen, J., Sanderson, B., Strickler, J. R. and Okubo, A. (1991) Feeding currents and energy dissipation by *Euchaeta rimana*, a subtropical pelagic copepod. *Limnol. Oceanogr.*, **36**, 362–369.

Yen, J., Weissburg, M. J. and Doall, M. H. (1998) The fluid physics of signal perception by mate-tracking copepods. *Phil. Trans. R. Soc. Lond.*, **B353**, 787–804.

Yule, A. B. and Crisp, D. J. (1983) A study of feeding behaviour in *Temora longicornis* (Müller) (Crustacea: Copepoda). *J. Exp. Mar. Biol. Ecol.*, **71**, 271–282.

*Received on October 20, 2000; accepted on September 7, 2001*